

RESEARCH ARTICLE

Regulation of dendrite growth and maintenance by exocytosis

Yun Peng^{1,*}, Jiae Lee^{1,*}, Kimberly Rowland², Yuhui Wen², Hope Hua², Nicole Carlson², Shweta Lavania², Jay Z. Parrish^{1,‡} and Michael D. Kim^{2,‡}

ABSTRACT

Dendrites lengthen by several orders of magnitude during neuronal development, but how membrane is allocated in dendrites to facilitate this growth remains unclear. Here, we report that *Ras opposita* (*Rop*), the *Drosophila* ortholog of the key exocytosis regulator *Munc18-1* (also known as *STXBP1*), is an essential factor mediating dendrite growth. Neurons with depleted *Rop* function exhibit reduced terminal dendrite outgrowth followed by primary dendrite degeneration, suggestive of differential requirements for exocytosis in the growth and maintenance of different dendritic compartments. *Rop* promotes dendrite growth together with the exocyst, an octameric protein complex involved in tethering vesicles to the plasma membrane, with *Rop*–exocyst complexes and exocytosis predominating in primary dendrites over terminal dendrites. By contrast, membrane-associated proteins readily diffuse from primary dendrites into terminals, but not in the reverse direction, suggesting that diffusion, rather than targeted exocytosis, supplies membranous material for terminal dendritic growth, revealing key differences in the distribution of materials to these expanding dendritic compartments.

KEY WORDS: Dendrite, *Drosophila*, Exocyst, Munc18-1, Neurodegeneration, STXBP1

INTRODUCTION

Axons and dendrites lengthen by several orders of magnitude during neuronal development, and this lengthening of neurites is essential for establishing the morphological features of a neuron that ultimately determine its connectivity and function. The addition of membrane proteins and lipids through exocytosis plays a fundamental role in this process, but growth in axons and dendrites appears to be regulated by distinct pathways. In *de novo* axon outgrowth, addition of new membrane occurs primarily through exocytosis of plasmalemmal precursor vesicles (PPVs) at the growth cone (Bray, 1970; Craig et al., 1995; Lockerbie et al., 1991), which is mediated, in part, by soluble N-ethylmaleimide-sensitive factor attachment protein receptor (SNARE) proteins (Pfenninger, 2009). PPVs that are synthesized in the cell body are transported to growing axons (Pfenninger and Johnson, 1983), and although the source for material to support dendrite growth is unclear, the polarized localization of satellite secretory pathways in dendrites suggests that PPVs might be locally generated in some dendrites (Horton et al., 2005; Pfenninger, 2009; Ye et al., 2007). Although it has been demonstrated that disrupting post-Golgi trafficking can impede dendrite growth (Horton et al., 2005; Ye

et al., 2007), little is known about the role that exocytosis specifically plays in dendritic morphogenesis.

Most intracellular membrane fusion events require both SNARE and Sec1/Munc18 (SM) proteins. SM-family proteins are essential components of the molecular machinery that regulates exocytosis and cooperate closely with SNARE proteins to mediate vesicle fusion (Sudhof and Rothman, 2009). Munc18-1 (also known as syntaxin binding protein 1, STXBP1), the neuron-specific isoform of the SM protein family, is a key regulator of neurosecretion and mediates synaptic vesicle release through its interactions with syntaxin-1 and the SNARE complex (Hata et al., 1993; Verhage et al., 2000). However, Munc18-1 protein is not restricted to axon terminals but is distributed throughout neurons, suggesting that Munc18-1 might have other roles in the neuronal membrane that are separable from its function in neurotransmitter release (Garcia et al., 1995).

In yeast, the SM protein Sec1 physically interacts with subunits of the exocyst to facilitate SNARE-complex assembly and membrane fusion upon vesicle arrival at the plasma membrane (Morgera et al., 2012; Wiederkehr et al., 2004). The exocyst is an evolutionarily conserved octameric protein complex that was originally identified in yeast based on its role in the spatial targeting and tethering of post-Golgi vesicles to specific sites of membrane expansion (Novick et al., 1980; TerBush et al., 1996). In the absence of a functional exocyst, secretory vesicles are delivered to the plasma membrane, but SNARE complexes do not form and exocytosis is blocked (Grote et al., 2000). Although the exocyst plays well-established roles in neuronal polarization and the regulation of neurite outgrowth (Hazuka et al., 1999; Lalli and Hall, 2005; Murthy et al., 2003; Vega and Hsu, 2001), a role in dendrite development has not been specifically attributed to the exocyst. Likewise, whether Sec1–exocyst complexes form in higher eukaryotes is unknown.

Drosophila class IV dendritic arborization (C4da) neurons elaborate highly complex dendritic arbors that undergo a period of extensive growth during larval development, during which time the linear dimensions of dendrites increase more than tenfold (Grueber et al., 2002; Parrish et al., 2009), necessitating enormous amounts of material to drive the expansion of the plasma membrane. C4da neurons therefore provide an excellent system to investigate how new material is supplied in dendrites to support their growth and maturation. Here, we identify *Rop*, the *Drosophila* homolog of vertebrate Munc18-1, as a key regulator of dendrite development. In *Rop* mutants, C4da neurons show an initial defect in outgrowth of terminal dendritic branches, followed by progressive loss of terminal dendrites and degeneration of major dendritic branches. We found that *Rop* mediates dendrite growth, in part, through interaction with the exocyst subunit Sec6. These *Rop*–Sec6 complexes are enriched in the primary dendrites of C4da neurons, suggesting that this dendritic compartment is the predominant site for dendritic exocytosis. Indeed, using a pH-sensitive *in vivo* reporter, we found that exocytosis predominates along major

¹Department of Biology, University of Washington, Seattle, WA 98195, USA.

²Department of Molecular and Cellular Pharmacology, University of Miami, Miller School of Medicine, Miami, FL 33136, USA.

*These authors contributed equally to this work

‡Authors for correspondence (jzp2@uw.edu; mkim2@med.miami.edu)

branches during dendrite arbor expansion and that the lateral diffusion of material from primary dendrites to terminal dendritic branches is likely to support terminal dendrite growth. Finally, we demonstrate that the balance between exocytosis and endocytosis is not only important for dendrite growth, but is also required for maintenance of the dendritic arbor.

RESULTS

Identification of *Rop* as a critical regulator of dendrite growth

To identify regulators of dendrite growth, we performed an RNA interference (RNAi)-based screen of phylogenetically conserved genes in class I da (C1da) neurons, which elaborate simple, stereotyped dendrites and are amenable to RNAi-based analysis of dendrite morphogenesis (Foley and O'Farrell, 2004; Parrish et al., 2006). From this screen, we found that double-stranded RNA (ds) RNA-mediated knockdown of *Rop* caused severe reductions in dendritic outgrowth of embryonic C1da neurons (data not shown). To validate the observed RNAi phenotype, we examined C1da neurons in embryos homozygous for an amorphic allele of *Rop* (*Rop*^{G27}) and found that C1da neurons in *Rop*^{G27} homozygous mutant embryos exhibited growth defects comparable to those upon *Rop* knockdown by using RNAi, including severe reduction in outgrowth of both the primary dendrite and secondary lateral branches (Fig. 1A,B), demonstrating that *Rop* is required for overall dendritic arbor growth. To explore the generality of *Rop* function in dendrite growth, we assayed for requirements of *Rop* function in the development of the more complex dendritic arbors of C4da neurons. Similar to C1da neurons, C4da neurons exhibited severe deficits in the outgrowth of primary dendrites and terminal dendritic branches in *Rop*^{G27} homozygous mutants, resulting in dramatic reductions in receptive field size (Fig. 1C,D). Thus, *Rop* appears to be generally required to support dendrite growth from early stages of dendrite development in the *Drosophila* embryonic peripheral nervous system (PNS). Consistent with *Rop* functioning in a cell-autonomous manner in dendrite growth, we found that *Rop* is highly expressed in multidendritic (md) sensory neurons, including all da neurons, during embryogenesis. However, *Rop* is also highly expressed in other cell types in the body wall, including the epidermis, suggesting that the function of *Rop* is not exclusive to neurons (Fig. 1E–G).

Rop is autonomously required for growth and maintenance of the dendritic arbor

Rop^{G27} mutants fail to develop normally beyond mid-embryogenesis, failing to produce cuticle and exhibiting abnormalities in the underlying epidermis (Harrison et al., 1994). Given the importance of non-autonomous epithelial-derived cues in influencing dendrite growth (Jiang et al., 2014; Parrish et al., 2009) and the broad distribution of *Rop* expression (Fig. 1E–G), we sought to assay for cell-autonomous functions of *Rop* in dendrite development. To this end, we performed mosaic analysis with a repressible cell marker (MARCM) to generate single-cell C4da neuron clones homozygous for the *Rop*^{G27} allele in an otherwise heterozygous background and assayed for effects on dendrite growth (Lee and Luo, 1999). Using *sensory organ precursor (SOP)-FLP* lines to facilitate the generation of C4da MARCM clones and reduce the impact of heat shock on developmental timing (Shimono et al., 2014), we found that dendrite defects were first manifest at 72 h after egg laying (AEL) in *Rop*^{G27} mutant C4da neuron clones (Fig. 2A). Although there was no statistical difference in the number of terminal dendritic branches or total dendrite length between *Rop* mutant and wild-type control neurons

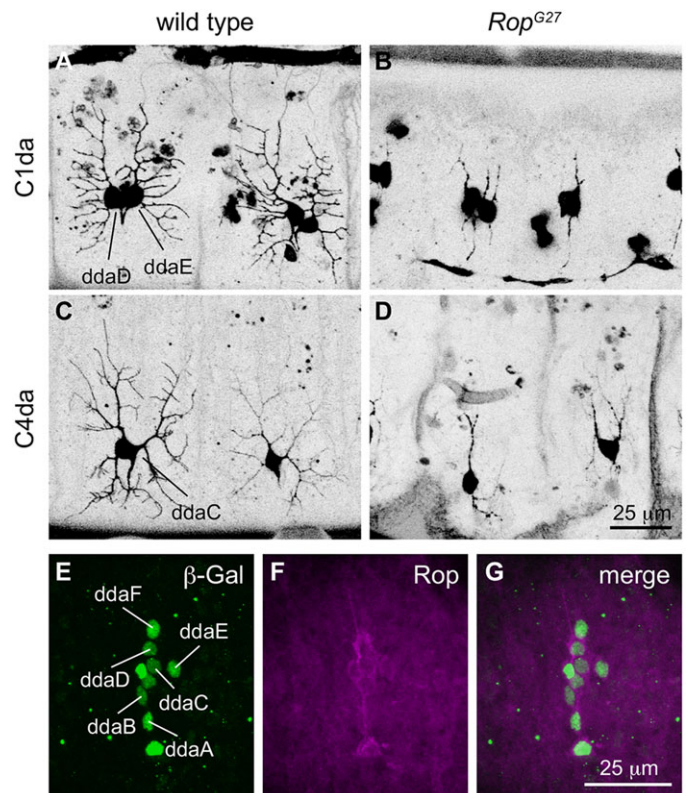


Fig. 1. *Rop* regulates dendrite growth. (A) Dendritic morphologies of wild-type dorsal class I da (C1da) neurons ddaD and ddaE in a late-stage embryo. (B) C1da neurons in a *Rop*^{G27} homozygous mutant exhibit reduced outgrowth of the primary dendrite and absence of lateral branching. (C) Dendritic morphology of wild-type dorsal class IV da (C4da) neuron ddaC in a late-stage embryo. (D) ddaC neurons in a *Rop*^{G27} homozygous mutant exhibit reduced primary dendrite outgrowth and lateral branching defects. (E–G) Multidendritic (md) neurons in a late-stage embryo labeled by the *E7-2-36 lacZ* enhancer trap line and revealed by staining for β-galactosidase (β-Gal, E) and with an antibody against *Rop* (F). *Rop* is expressed in all da neurons in the dorsal cluster (G). Anterior is to the left, and dorsal is up in this and all subsequent figures.

(Fig. 2B), a noticeable thinning of terminal dendrites in *Rop* mutant C4da neurons was apparent at this time point. By 96 h AEL, *Rop*^{G27} C4da MARCM clones exhibited severely reduced dendritic complexity, as indicated by significant reductions in total dendrite length and in the total number of terminal dendritic branches (Fig. 2A,B). This reduction in complexity in the *Rop* mutant was not due to an overall loss of dendrites, as the numbers of terminal dendrites in *Rop* mutants did not differ significantly at 72 h and 96 h AEL, and is more likely to reflect a failure in dendritic branch formation. Varicosities along some of the major dendritic branches also become apparent by this time (Fig. 2A, arrows). By 144 h AEL, *Rop*^{G27} C4da MARCM clones showed a profound loss of dendrites and extensive beading along the major dendritic branches. In extreme cases, *Rop* mutant neurons were completely devoid of terminal dendritic branches, and primary dendrites appeared highly fragmented, features that are characteristic of dendrite degeneration (Fig. 2C). We further monitored the effects of *Rop* mutations on axon growth by visualizing axon projection patterns of individual da neuron MARCM clones. Although *Rop*^{G27} C4da MARCM clones exhibited severe defects in dendritic morphology at 96 h AEL, there was no obvious abnormality in the axon projections of *Rop* mutant da neuron clones at this time point (data not shown). However, axons of *Rop* mutant neurons

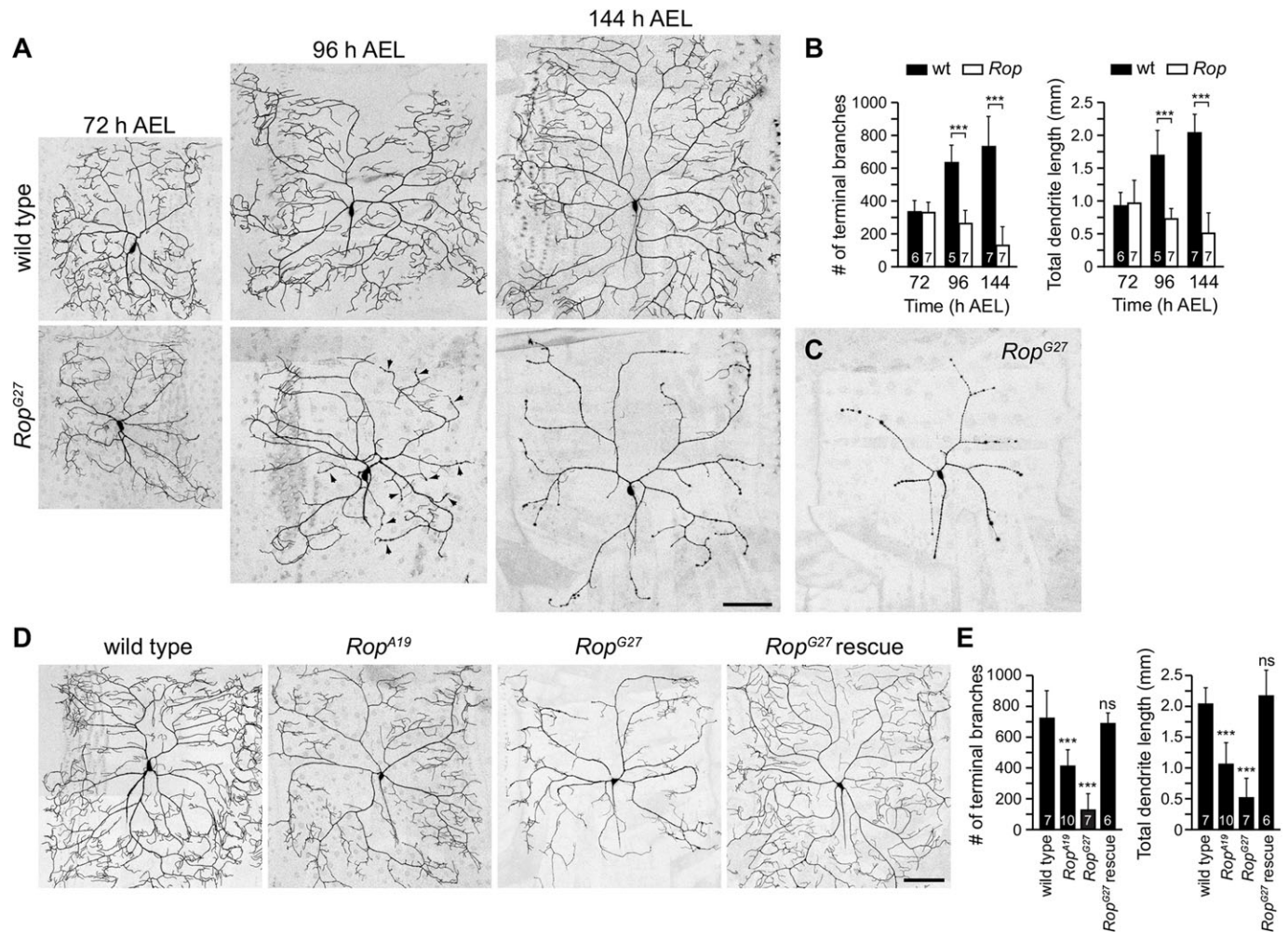


Fig. 2. Differential requirements for the function of *Rop* in dendrite growth. (A) Dendritic morphologies of representative wild-type or *Rop^{G27}* C4da MARCM clones at indicated time points. Arrowheads mark varicosities on dendrite branches. Clones were imaged live, and all images are shown at the same magnification. (B) Quantification of the total number of terminal dendrite branches and the total dendrite length in wild-type or *Rop^{G27}* mutant C4da-ddaC MARCM clones at the indicated times. The number of clones analyzed for each time point and genotype combination is indicated. *** $P < 0.001$ [one-way ANOVA with Tukey's honest significant difference (HSD) post-hoc analysis]. (C) At 144 h AEL, 4 out of 19 *Rop^{G27}* mutant C4da-ddaC MARCM clones analyzed exhibited a total loss of terminal dendrites and extensive fragmentation of major dendrites. (D) Dendritic morphologies of representative wild-type, *Rop^{A19}*, *Rop^{G27}*, or *Rop^{G27} rescue* (*Rop^{G27} + UAS-NYFP-Myc-Rop*) C4da-ddaC MARCM clones at 144 h AEL. (E) Quantification of the total number of terminal dendrite branches and the total dendrite length, with the number of neurons analyzed for each genotype indicated. *** $P < 0.001$; ns, not significant compared to wild-type controls (one-way ANOVA with Tukey's HSD post-hoc analysis). Means \pm s.d. are shown. Scale bars: 100 μ m (A,D).

appeared thin with varicosities along the terminals by 144 h AEL (Fig. S1), suggesting that *Rop* might also be required for some aspects of axon development.

The dendrite phenotypes we observed could reflect a role for *Rop* in dendrite growth or could be a secondary effect of cell death caused by loss of *Rop* function. To differentiate between these two possibilities, we stained *Rop^{G27}* C4da MARCM clones with markers of cell death and found that *Rop* mutant clones showed no detectable signal for the apoptotic effector Death caspase-1 (Dcp-1), and excluded the vital dye Acridine Orange (Fig. S1; data not shown). To further establish the requirement for *Rop* function in dendrite patterning, we monitored the effects of a second *Rop* allele (*Rop^{A19}*) on dendrite growth. Similar to what we observed with the *Rop^{G27}* allele, C4da MARCM clones homozygous for the hypomorphic *Rop^{A19}* allele showed significant reductions in total dendrite length and in the total number of terminal dendritic branches (Fig. 2D,E). Finally, we found that expressing an epitope-tagged version of *Rop* was sufficient to rescue the dendrite growth

defects of *Rop* mutants (Fig. 2D,E), further demonstrating that *Rop* functions in a cell-autonomous manner in C4da neurons to promote dendrite growth.

Given the severity of the dendritic growth defect in *Rop^{G27}* homozygous mutant embryos, we examined whether *Rop* protein perdurance contributed to the delayed phenotype of *Rop^{G27}* mutant MARCM clones. Indeed, immunoreactivity of *Rop* was detectable in *Rop^{G27}* mutant C4da MARCM clones at 72 h AEL, when dendrite defects first become apparent, whereas immunoreactivity of *Rop* was dramatically reduced in *Rop^{G27}* mutant C4da MARCM clones at 120 h AEL (Fig. S2). Similarly, perdurance of maternal *Rop* function masks embryonic phenotypes in zygotic *Rop* mutants (Harrison et al., 1994). Thus, the late onset of dendrite defects is likely to reflect the timing of *Rop* activity exhaustion in *Rop^{G27}* MARCM clones, with persistent *Rop* protein supporting dendrite growth up to 72 h AEL. Interestingly, the growth defects were not uniformly distributed in dendrite arbors of *Rop^{G27}* mutant C4da clones – terminal dendrites exhibited heightened sensitivity to *Rop*

function, suggesting that terminal dendrites have an increased requirement for exocytosis compared to other regions of the arbor, that exocytic membrane addition preferentially occurs at terminal dendrites, or both. To further explore the generality of the role of exocytosis in dendrite growth, we monitored the effects of RNAi-mediated knockdown of a subset of SNARE proteins that are important for vesicle trafficking and fusion, including *Syntaxin1A*, *Snap24*, *Snap25*, α -*SNAP* and *Synaptotagmin 1*. Knockdown of these components led to significant reductions in terminal branching (Fig. S3), consistent with the notion that terminal dendrites have a heightened requirement for the exocytic machinery. Taken together, our results indicate a role for the exocytic machinery in dendritic morphogenesis and demonstrate a cell-autonomous requirement for *Rop* in the growth and subsequent maintenance of the dendritic arbor.

Rop interacts with the exocyst to control dendritic branching

We next set out to identify genes that act with *Rop* to control dendritic morphogenesis, focusing our attention on the possible relationship between *Rop* and the exocyst, which regulates polarized trafficking of membranous material. To determine whether the exocyst is required in a cell-autonomous manner for dendrite morphogenesis, we used MARCM to generate C4da neuron clones that were homozygous mutant for loss-of-function alleles of two core components of the exocyst complex – *Sec5* (*Sec5^{E10}*) and *Sec6* (*Sec6^{Ex15}*) (Murthy et al., 2003, 2005). We found that both *Sec5^{E10}* and *Sec6^{Ex15}* C4da MARCM clones showed significant reductions in the total numbers of terminal dendritic branches as well as total dendrite length (Fig. 3A–E), demonstrating a cell-autonomous function of the exocyst in dendrite growth. Furthermore, consistent with *Sec5* and *Sec6* functioning together in dendrite development, Sholl analysis revealed a remarkable phenotypic similarity between C4da neurons deficient for *Sec5* or *Sec6* (Fig. 3F). Of note, a comparable reduction in the number of dendritic intersections was observed in *Rop^{G27}* C4da MARCM clones (data not shown). Outgrowth of the major dendritic branches was only moderately affected in the exocyst mutants because the primary dendrites of *Sec5^{E10}* and *Sec6^{Ex15}* C4da MARCM clones extended to the dorsal midline and segment borders (Fig. 3B,C). However, varicosities along portions of major dendrites and thinning of terminal dendrites were apparent in *Sec5* and *Sec6* mutant clones (Fig. 3B,C), a phenotype reminiscent of *Rop^{G27}* C4da MARCM clones.

Based on the phenotypic similarity of *Rop* and *Sec5* or *Sec6* mutants, we investigated whether *Rop* and the exocyst function together in dendrite development. First, we determined whether *Rop* interacts genetically with *Sec5* and/or *Sec6* in the control of dendrite morphogenesis. Dosage-dependent genetic interactions are often indicative of a shared function in C4da neuron dendrite development (Parrish et al., 2007), therefore we assayed for dendrite growth defects in larvae with trans-heterozygous combinations of *Rop^{G27}* with the *Sec5^{E13}* or *Sec6^{Ex15}* allele (Fig. 3G–L). Indeed, trans-heterozygous combination of *Rop^{G27}* with *Sec5^{E13}* resulted in reduced numbers of terminal dendritic branches compared to C4da neurons in *Rop^{G27/+}* and *Sec5^{E13/+}* heterozygotes ($P=0.06$; *Sec5^{E13/+}*; *Rop^{G27/+}* trans-heterozygotes versus *Sec5^{E13}* heterozygotes). We also found that C4da neurons in *Sec6^{Ex15/+}*; *Rop^{G27/+}* trans-heterozygotes exhibited significant reductions in terminal dendritic branching compared to C4da neurons in *Rop^{G27/+}* and *Sec6^{Ex15/+}* heterozygotes alone ($P<0.05$) (Fig. 3M). Thus, *Rop* genetically interacts with *Sec5* and *Sec6* to regulate dendrite development.

Because *Rop* genetically interacts with genes encoding exocyst subunits to regulate dendritic branching, we next tested whether *Rop* can physically associate with individual exocyst subunits *in vivo*. We performed co-immunoprecipitation experiments using a monoclonal antibody against *Rop* and found that *Rop* co-immunoprecipitated with endogenous *Sec6* from adult *Drosophila* whole-brain extracts, as revealed by western blotting with an antibody against *Sec6* (Fig. 3N). We further found that *Rop* co-immunoprecipitated with endogenous *Sec15* from whole-brain extracts (Fig. 3N). Thus, *Rop* forms complexes with exocyst subunit proteins *in vivo*. Taken together, these data suggest that *Rop* can associate with multiple subunits of the exocyst complex, and that *Rop* and exocyst genes are likely to function in the same pathway to control dendritic morphogenesis.

Exocytosis preferentially occurs along primary dendrites

During larval development, terminal dendrite growth and addition accounts for the majority of C4da dendrite growth (Fig. 4A,B). Our finding that mutations in *Rop* and exocyst subunits preferentially affected growth and maintenance of terminal dendrites during larval development suggests that growing terminal dendrites might be the primary target for exocytosis during neuronal growth. If this is the case, we reasoned that the exocytic machinery would be preferentially localized to terminal dendrites. To address this possibility, we monitored the endogenous distribution of *Rop* in larval C4da neurons using a monoclonal antibody to *Rop* (Harrison et al., 1994). Although we observed *Rop* immunoreactivity in major dendritic branches, the *Rop* signal was not detectable or much weaker at terminal dendrites of C4da neurons (Fig. 4C–E). However, *Rop* immunoreactivity was present throughout the body wall, precluding high-resolution analysis of *Rop* distribution in terminal dendrites. To circumvent this problem, we expressed an epitope-tagged version of *Rop* (Myc-*Rop*) in C4da neurons. As with endogenous *Rop*, epitope-tagged *Rop* was enriched in major dendrites; a weak signal was present in some higher order dendrites but rarely extended the entire length of terminal dendrites (Fig. 4F–H). We conclude that the distribution of *Rop* is not uniform in C4da dendrite arbors and appears to be predominantly localized to major dendrites.

It is possible that the exocyst spatially restricts the localization of assembled SNARE complexes (Carr et al., 1999; Grote et al., 2000; Wiederkehr et al., 2004), and in this manner, tethers *Rop* to specific sites of exocytosis. We reasoned that if the exocyst accumulates at terminal dendrites, then it might efficiently recruit *Rop* to terminal dendrites, even though the majority of *Rop* is restricted to major dendrites. To test this possibility, we monitored exocyst distribution in C4da neurons by co-expressing a GFP-tagged version of *Sec15*, which has been previously used to visualize the exocyst (Jafar-Nejad et al., 2005), in C4da neurons also expressing the CD4–tdTomato membrane marker. Interestingly, we observed that *Sec15*–GFP is enriched in the soma, where it accumulates in large punctate structures, and is also distributed along major dendrites with notable accumulations at dendritic branch points (Fig. 4I–K). As with *Rop*, *Sec15*–GFP was present at much lower levels in terminal dendrites. Therefore, our data suggest that the exocytic machinery is enriched in major dendrites.

The distribution of *Rop* and exocyst components in C4da dendrites suggests that dendritic exocytosis occurs primarily along the major dendritic branches rather than at terminal dendrites. To test this possibility, we used two imaging-based approaches. First, we reasoned that visualization of *Rop*–exocyst complex formation

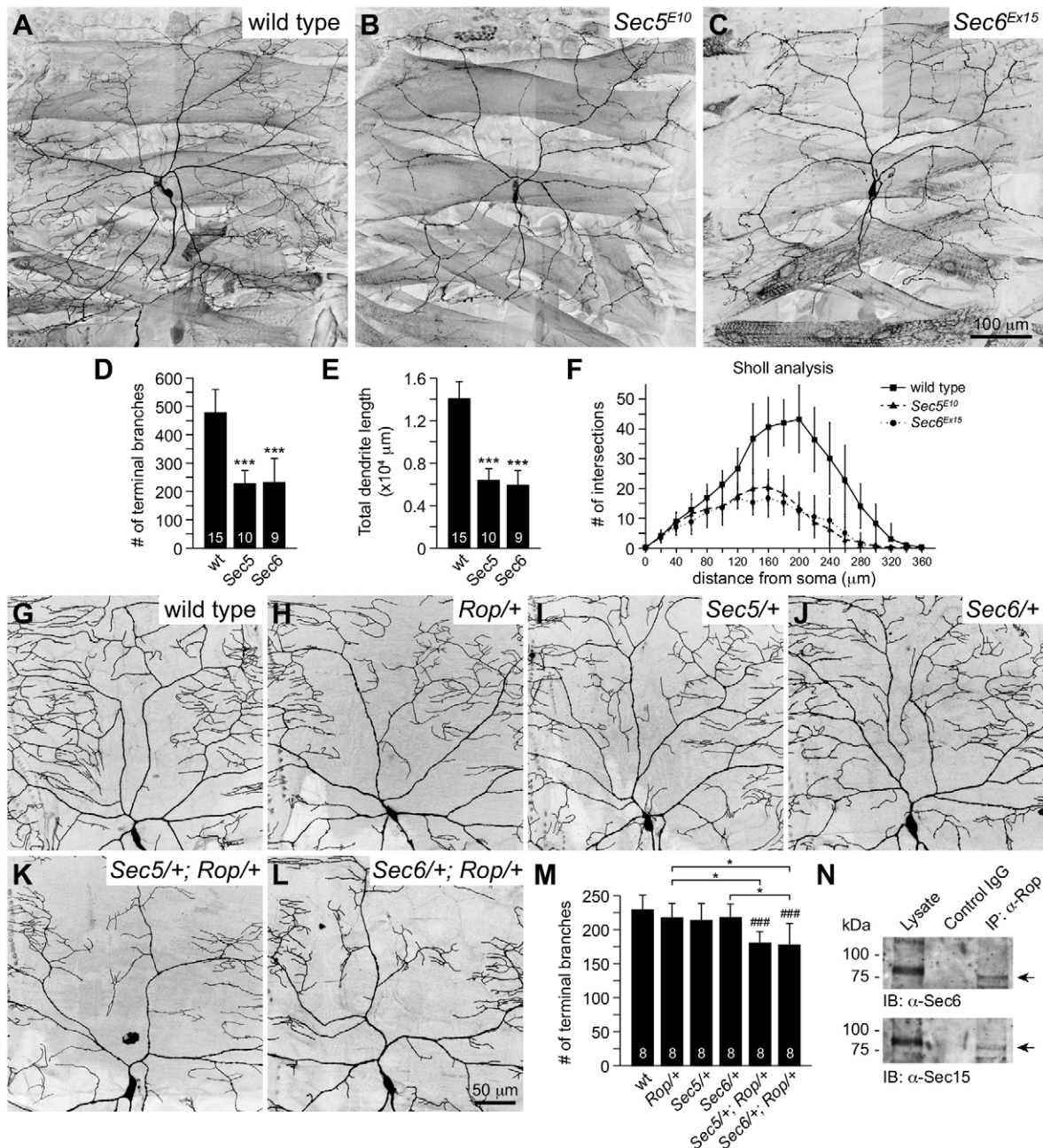


Fig. 3. Rop interacts with the exocyst complex. (A–C) Dendritic morphology of a wild-type (A), *Sec5^{E10}* (B) or *Sec6^{Ex15}* (C) C4da-ddaC MARCM clone in a fixed preparation of late-stage third instar larva. (D,E) Quantification of the total number of terminal dendrite branches (D) and total dendrite length (E) in wild-type, *Sec5^{E10}* and *Sec6^{Ex15}* C4da-ddaC MARCM clones. *** $P < 0.001$ (one-way ANOVA with Tukey's HSD post-hoc analysis). (F) Sholl analysis of wild-type, *Sec5^{E10}* and *Sec6^{Ex15}* C4da-ddaC MARCM clones. FRT40A and FRT42D control clones were pooled as wild type in (D–F) for the purposes of statistical analysis. (G–L) Dendritic morphology of a C4da-ddaC neuron in a wild-type (G), *Rop^{G27/+}* heterozygous (H), *Sec5^{E13/+}* heterozygous (I), *Sec6^{Ex15/+}* heterozygous (J), *Sec5^{E13/+}; Rop^{G27/+}* trans-heterozygous (K) and *Sec6^{Ex15/+}; Rop^{G27/+}* trans-heterozygous third instar larva at 144 h AEL (L). All neurons were imaged live. (M) Quantification of the total number of terminal dendritic branches per $10.1 \times 10^4 \mu\text{m}^2$ field. *Statistical comparison to wild type; * $P < 0.05$, ### $P < 0.001$ (one-way ANOVA with Tukey's HSD post-hoc analysis). (N) Rop forms a complex with exocyst components Sec6 and Sec15. Co-immunoprecipitation using Rop monoclonal antibody 4F8 precipitates Sec6 and Sec15 from adult whole-brain lysates, as detected by immunoblotting. Arrow indicates Sec6 protein (top) and Sec15 protein (bottom). Means \pm s.d. are shown. D,E,M, the number of neurons analyzed for each genotype are indicated.

in vivo would allow us to identify sites of vesicle–plasma-membrane attachment. To this end, we used bimolecular fluorescence complementation (BiFC), in which two interacting proteins are fused to two non-fluorescent fragments of yellow fluorescent protein (YFP), the N-terminal (NYFP) and C-terminal (CYFP) fragments (Gohl et al., 2010; Hu et al., 2002). In this assay, binding

of the interacting proteins facilitates YFP reconstitution, thus YFP fluorescence serves as a proxy for tracking protein–protein interactions *in vivo*. Reassembly of split YFP is irreversible *in vitro* (Hu et al., 2002), so BiFC should provide a cumulative record of Rop–exocyst complex formation and hence facilitate visualization of complexes throughout the cell.

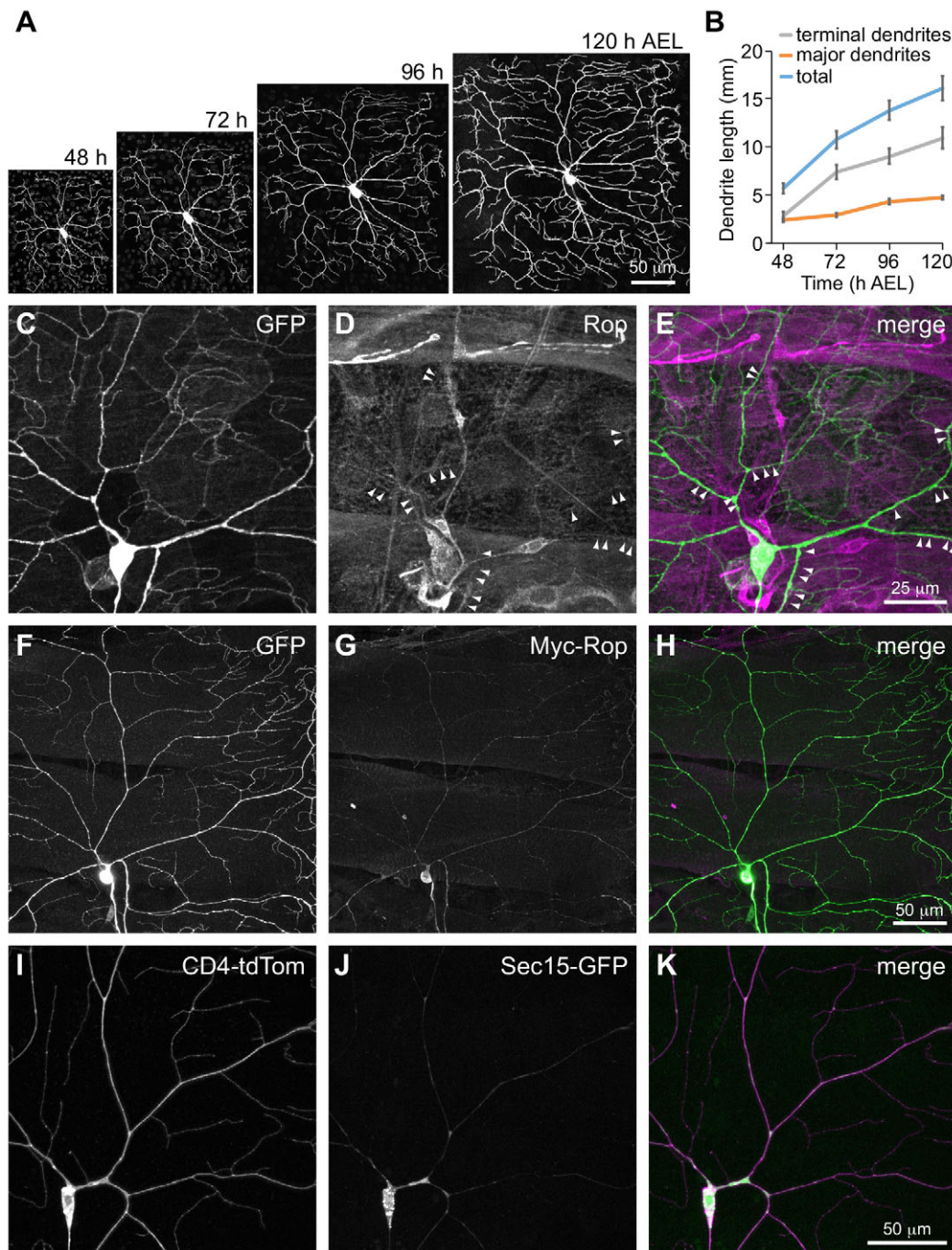


Fig. 4. Exocytic machinery preferentially localizes to major dendrites. (A,B) Time-lapse imaging of dendrite growth in larval C4da neurons. (A) A representative individual C4da neuron (positively labeled using MARCM) is shown at the indicated time points. (B) Mean values and s.d. for total dendrite length, terminal dendrite length and primary dendrite length for five ddaC MARCM clones imaged at each time point. (C–E) GFP (to mark C4da neurons, green) and Rop immunostaining (magenta) of a *ppk-EGFP* third instar fillet reveals prominent Rop immunoreactivity in major dendrites (arrowheads). (F–H) Images of a third instar larva expressing GFP and epitope-tagged Rop (NYFP–Myc–Rop) specifically in C4da neurons immunostained with antibodies against GFP and Myc. (I–K) The exocyst is enriched in major dendrites and accumulates at dendritic branch points. Live images of a third instar larva expressing tdTomato and GFP-tagged Sec15 specifically in C4da neurons.

Yeast Sec1 and Sec6 can directly interact *in vitro* (Morgera et al., 2012), and we found that Rop and Sec6 co-immunoprecipitate in *Drosophila* neurons (Fig. 3N), therefore we examined whether Rop and Sec6 directly interact in *Drosophila* S2 cells. First, as a negative control, we co-expressed the two halves of split YFP (CYFP and NYFP) in S2 cells and observed no detectable YFP fluorescence (Fig. S4), demonstrating that interacting proteins are required for

efficient YFP reassembly. Next, we generated both N- and C-terminal fusions of Rop with NYFP, and N- and C-terminal fusions of Sec6 with CYFP, and tested for YFP reconstruction in S2 cells. A strong BiFC signal was apparent only when NYFP–Rop was transfected with Sec6–CYFP, demonstrating the specificity of the interaction (Fig. S4). Thus, we conclude that Rop and Sec6 can directly interact in *Drosophila* S2 cells.

Using NYFP–Rop and Sec6–CYFP, we next monitored complex formation between Rop and Sec6 in the *Drosophila* larval body wall. First, we assayed for *in vivo* function of NYFP–Rop and Sec6–CYFP. We expressed *UAS-NYFP-Rop* in *Rop* mutant C4da MARCM clones and *UAS-Sec6-CYFP* in *Sec6* mutant C4da MARCM clones, and found that both transgenes rescued the respective mutant phenotypes (Fig. 2D,E; Fig. S4). These results indicate that NYFP–Rop and Sec6–CYFP are functional proteins, and suggest that the BiFC signal is likely to reflect the normal localization of Rop–Sec6 complexes *in vivo*. Sec6 complexes localize to basolateral junctional domains in polarized epithelial cells where they appear to mediate polarized delivery of cargo (Grindstaff et al., 1998), therefore we next examined whether the Rop–Sec6 BiFC signal accumulates at junctional domains in the larval epidermis. Indeed, co-expression of NYFP–Rop with Sec6–CYFP using the epidermal *A58-Gal4* driver yielded robust YFP reconstitution in body wall epithelial cells, with Rop–Sec6 complexes enriched at junctional domains (Fig. S4). Finally, we assayed for Rop–Sec6 complex formation in C4da neurons. When we co-expressed NYFP–Rop and Sec6–CYFP in C4da neurons, we observed strong YFP fluorescence in major dendrites but little or no signal in terminal dendrites (Fig. 5A,B), suggesting that the Rop–exocyst interaction, and hence vesicle tethering to the plasma membrane, primarily occurs in major but not terminal dendrites. In contrast to the dendritic distribution of Rop–Sec6 complexes, co-expressing NYFP–Rop and Sec6–CYFP yielded robust YFP reconstitution in C4da axon terminals (Fig. 5C), consistent with previous reports that the exocyst is required for exocytosis of Golgi-derived vesicles in axon terminals of *Drosophila* motor neurons (Murthy et al., 2003, 2005). Thus, the Rop–Sec6 complexes are differentially distributed in different compartments within C4da neurons – they are enriched in axon terminals and major dendrites but present only at low levels in terminal dendrites. These results

suggest that the capacity for exocytosis within C4da neurons is not uniform.

To more directly visualize sites of exocytosis and function, we utilized a pH-sensitive reporter (pHluorin-CD4-tdTomato; referred to as pH-Tom) comprising pH-sensitive GFP (ecliptic pHluorin) fused to the N-terminus of a red fluorescent membrane marker (CD4-tdTomato) (Kanamori et al., 2015) (Fig. 6A). The chromophore of ecliptic pHluorin is protonated at acidic pH (Miesenböck et al., 1998), hence pHluorin fluorescence is quenched within acidified intracellular compartments. As a result, the pH-Tom reporter fluoresces as both green and red at the cell surface but loses green fluorescence in acidified intracellular compartments, such as in exocytic vesicles. In cells expressing this reporter, regions with low levels of exocytosis should have reduced levels of green fluorescence compared to regions with high levels of exocytosis.

When we constitutively expressed pH-Tom in C4da neurons, beginning during late embryogenesis, we observed comparable ratios of green and red fluorescence throughout dendrite arbors in third instar larvae (Fig. 6B–D). However, over extended timescales, endocytosis and lateral diffusion might obscure regional differences in exocytosis as reported by pH-Tom. We therefore used a *Flp*-recombinase-inducible *ppk-Gal4* driver (Kanamori et al., 2013) to inducibly and selectively express pH-Tom in C4da neurons, reasoning that by tracking newly synthesized pH-Tom, we could more accurately monitor patterns of exocytic vesicle delivery. Using this approach, we found that the pH-Tom reporter accumulates to detectable levels approximately 24 h after induction of *Flp* expression. We therefore induced *Flp* expression at 48 h AEL and monitored pH-Tom fluorescence in C4da dendrites at 72 h AEL, the time at which dendrite defects were first apparent in *Rop* mutant C4da clones (Fig. 6E). Similar to what we observed following constitutive expression of the reporter, green (pHluorin) and red (Tomato) fluorescent signals were readily detectable in major

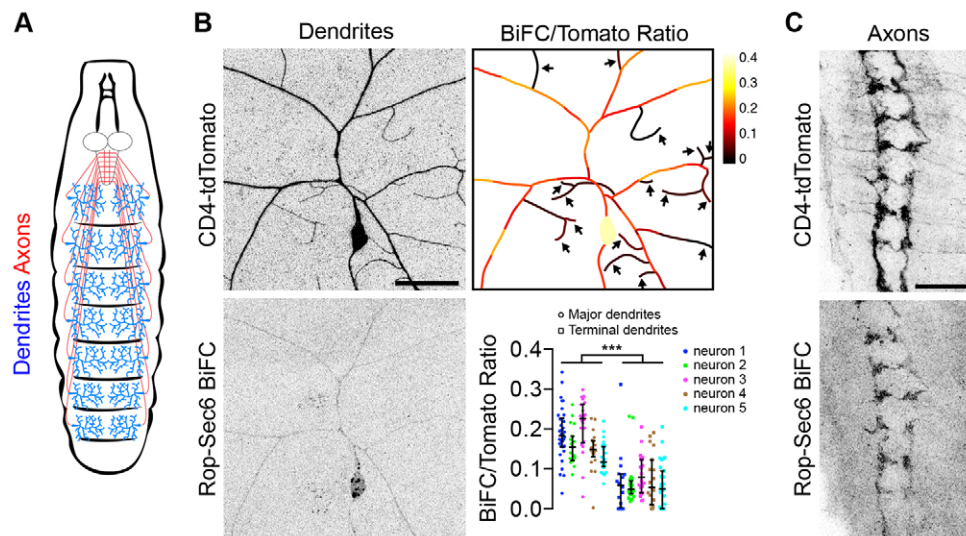


Fig. 5. Visualization of Rop–Sec6 complexes *in vivo*. (A) Schematic representation of C4da neurons in the larval peripheral nervous system. C4da axons project into the ventral nerve cord of the central nervous system. (B) Rop–Sec6 complexes preferentially localize to major branches in C4da dendrite arbors. Dendrite arbors of C4da neurons expressing *UAS-NYFP-Rop* together with *UAS-Sec6-CYFP* were labeled with *ppk-CD4-tdTomato*, and Rop–Sec6 complex formation was assayed by monitoring YFP fluorescence as (NYFP–Rop)–(Sec6–CYFP) interactions promote YFP reassembly (BiFC signal). Dendrite arbors were segmented into 15- μ m segments, and BiFC and CD4–tdTomato signal intensities were measured in 25 such segments of major dendrites and terminal dendrites. Ratios of BiFC:CD4–tdTomato signal are displayed according to a lookup table for one neuron (arrows mark terminal dendrites), and measurements are shown for five neurons (circles, major dendrites; squares, terminal dendrites). Bars mark median values and interquartile range. *** $P < 0.001$, paired *t*-test (comparing means of BiFC:tdTomato ratios in major dendrites and terminal dendrites). (C) The Rop–Sec6 BiFC signal was readily detectable in terminal arbors of C4da axons in the ventral nerve cord. Scale bars: 50 μ m (B); 25 μ m (C).

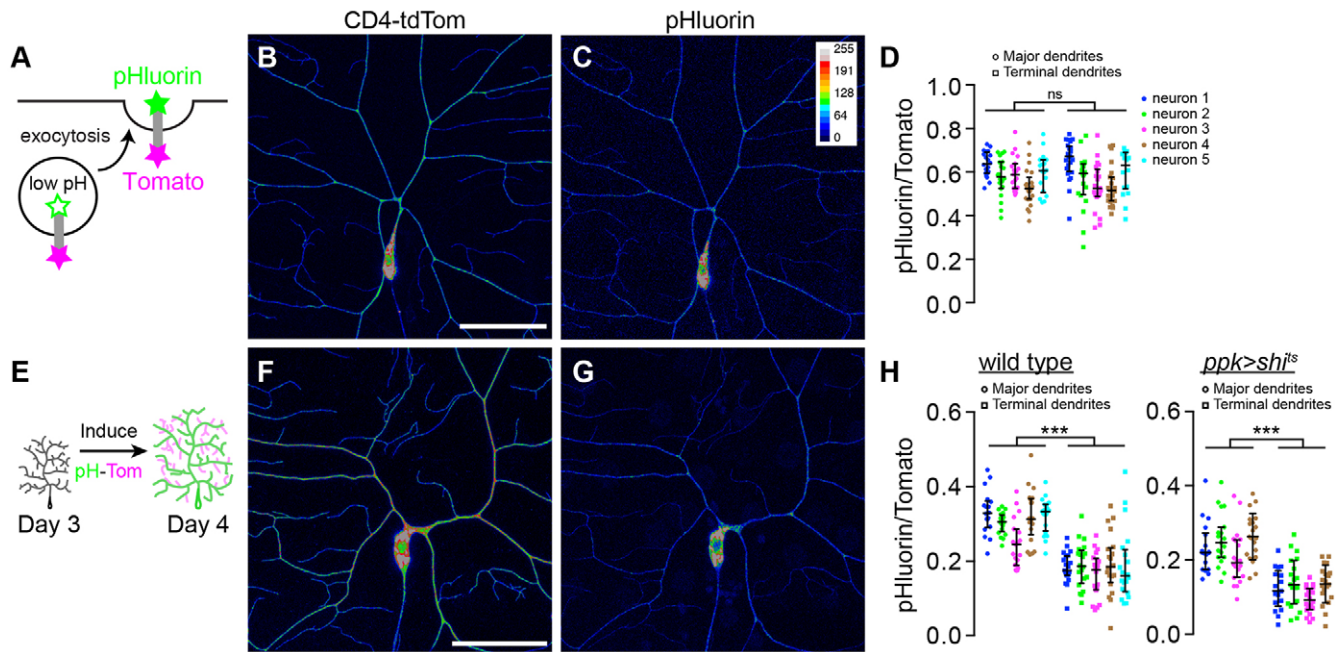


Fig. 6. Exocytosis preferentially occurs on major dendrites. (A) Schematic of pHluorin–CD4–tdTomato (pH-Tom) reporter, which has different fluorescent properties at acidic and neutral pH. (B) CD4–tdTomato and (C) pHluorin fluorescence at 96 h AEL following constitutive pH-Tom reporter expression in C4da neurons. Signal intensity is depicted according to a lookup table. Note that the pHluorin signal is detectable throughout the dendrite arbor. (D) Dendrite arbors were segmented into 15- μ m segments, and ratios of pHluorin and CD4–tdTomato signal intensities are shown for 25 such segments of major dendrites (circles) and terminal dendrites (squares) for each neuron analyzed. $n=5$ neurons. Bars mark median values and interquartile range. ns, not significant; $P>0.05$, paired t -test (comparing means of pHluorin:tdTomato ratios in major dendrites and terminal dendrites). (E) Schematic of the pulse–chase experiment to monitor exocytosis during dendrite growth. (F) CD4–tdTomato, (G) pHluorin fluorescence at 72 h AEL, and (H) fluorescence intensity measurements 24 h after induction of pH-Tom reporter expression in wild-type C4da neurons (left) or C4da neurons in which endocytosis was blocked during induction of pH-Tom reporter expression (*ppk>shi^{ts1}*; right). Larvae were raised at 29°C during the 24 h period following induction of Flp activity to block endocytosis. *** $P<0.001$, paired t -test (comparing means of pHluorin:tdTomato ratios in major dendrites and terminal dendrites). Scale bars: 50 μ m (B,F).

dendrite branches (Fig. 6F–H). However, compared to major dendrites, the ratio of green:red fluorescence was significantly reduced in terminal dendrites, suggesting that exocytosis preferentially occurs along major dendrites (Fig. 6H). Alternatively, these results could reflect heightened rates of endocytosis in terminal dendrites. However, we observed a similar distribution of pH-Tom fluorescence when we simultaneously induced pH-Tom expression and blocked endocytosis using a temperature-sensitive dominant-negative allele of *shibire* (*shi^{ts1}*) (Kitamoto, 2001) (Fig. 6H), suggesting that the absence of pHluorin fluorescence in terminal dendrites is not a consequence of endocytosis. Thus, although the pH-Tom reporter readily accumulates in terminal dendrites, pH-Tom is more efficiently delivered to the plasma membrane in major dendrites.

Our results thus far indicate that exocytosis occurs primarily along major dendrites, whereas the majority of dendrite growth occurs in terminal dendrites. We therefore investigated the possibility that material delivered to major dendrites might be supplied to terminal dendrites through diffusion to facilitate growth. If terminal dendrites rely on diffusion for materials to support membrane expansion, then diffusion of materials into terminals needs to occur at a faster rate than diffusion out of terminals. To examine this possibility, we monitored the dynamics of a membrane-associated protein in dendrites by measuring the lateral diffusion of a myristoylated photoactivatable fluorescent protein (myr-Eos) after photoconversion. Specifically, we photoconverted myr-Eos in major dendrites and monitored diffusion of the photoconverted protein in major dendrites and into terminal dendrites (Fig. 7A,B), or photoconverted myr-Eos in terminal dendrites and monitored diffusion within the terminals and into

major dendrites (Fig. 7C). Using this approach, we observed robust lateral diffusion of myr-Eos within major dendrites or within terminal dendrites, modest diffusion from major dendrites into terminals, and very little diffusion from terminals into main dendrites (Fig. 7B,C). Although the photoconverted myr-Eos is likely to comprise both cytosolic and membrane-bound forms of the fluorescent protein, a cytosolic version of Eos that is not membrane-bound freely diffused between the two compartments (Fig. 7B,C), suggesting that the directional bias in myr-Eos diffusion is primarily due to its association with the membrane. We next tested the possibility that mutations in *Rop* affect the dynamics of membrane proteins by monitoring diffusion of a membrane-targeted GFP (mCD8–GFP) in both wild-type and *Rop^{G27}* C4da MARCM clones using fluorescence recovery after photobleaching (FRAP). Notably, when we photobleached mCD8–GFP in terminal dendrites and assayed recovery from mCD8–GFP in major dendrites, we observed no difference between control and *Rop* mutant clones (Fig. 7D). Likewise, the recovery half-time and the percentage of fluorescence recovery in major dendrites were unchanged in *Rop* mutant neurons compared to that of wild-type controls (Fig. 7D), suggesting that lateral diffusion of membrane-associated proteins is not impaired when exocytosis is attenuated. Taken together, these results are consistent with the hypothesis that material delivered to primary dendrites by exocytosis diffuses into terminals to support terminal dendrite growth.

Blocking endocytosis mitigates dendrite growth defects of *Rop* mutants

At first glance, our findings that terminal dendrites have a heightened requirement for exocytic machinery and that exocytic

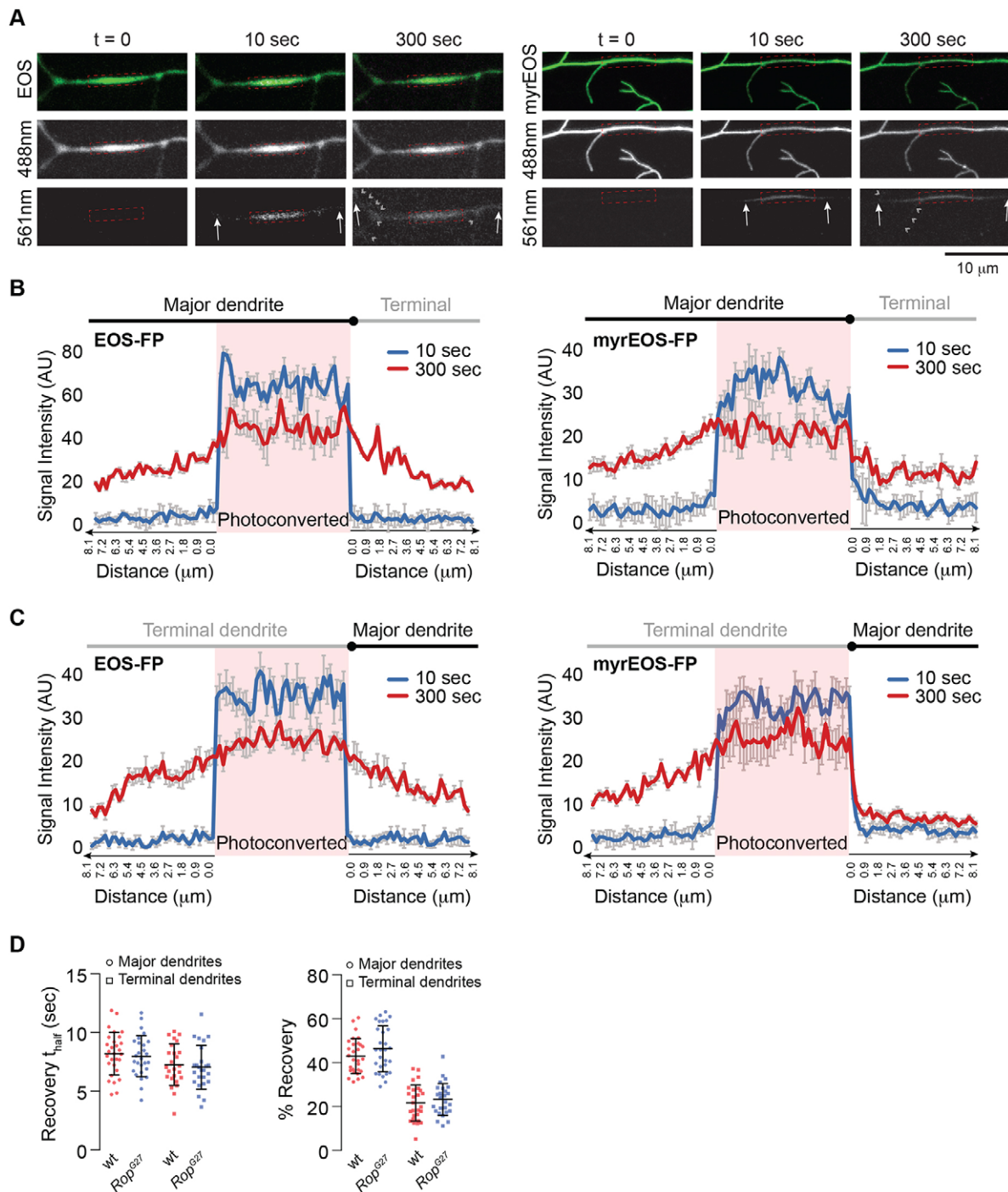


Fig. 7. Directional diffusion of membrane proteins into terminal dendrites. (A) Dendrites of a C4da neuron expressing photo-convertible cytosolic Eos or myr-Eos imaged before photo-conversion ($t=0$), 10 s after conversion in the region marked by the red hatched box ($t=10$ s) and 300 s after conversion ($t=300$ s). Green fluorescent myr-Eos (488-nm excitation) and photo-converted red fluorescent myr-Eos (561-nm excitation) are shown. Arrows mark the boundary of lateral diffusion within the dendrite branch, and double carats mark diffusion into terminal dendrites. Mean intensity of red fluorescent Eos (EOS-FP) or myr-Eos (myrEOS-FP) within an 8- μ m photo-converted region (B) on a major dendrite and 8- μ m neighboring regions on the same dendrite branch and in an adjacent terminal dendrite, or (C) in a terminal dendrite branch and 8 μ m neighboring regions on the same dendrite branch and in an adjacent major dendrite at 10 s and 300 s after photo-conversion. $n=8$ regions of interest, each from a different neuron, no more than two neurons were sampled from the same larva; error bars represent s.d. (D) FRAP analysis of membrane protein diffusion in *Rop^{G27}* mutant neurons. Plots shown mean values and s.d. for t_{half} (half-time of recovery) and percentage recovery for mCD8-GFP in 10 μ m ROIs within major dendrites, or within entire terminal dendrites of wild-type and *Rop^{G27}* mutant C4da MARCM clones. $n>25$ dendrites for each category and genotype pair.

machinery and activity are concentrated in primary dendrites seem at odds with one another. However, dendrites in many systems exhibit high rates of endocytic activity, and the balance of exocytosis and endocytosis is likely to be a crucial factor in

ensuring the proper development of the dendritic arbor (Blanpied et al., 2002; Parton et al., 1992). We therefore hypothesized that an imbalance in exocytosis and endocytosis contributes to the growth defect of terminal branches in *Rop* mutants. If this is the case, we

reasoned that blocking endocytosis might partially limit the terminal dendrite growth defects caused by depleted *Rop* function. To test this possibility, we selectively blocked endocytosis in C4da neurons by expressing *shi^{ts1}* in control and *Rop^{G27}* MARCM clones. Larvae with C4da MARCM clones were shifted to the non-permissive temperature for *shi^{ts1}* (30°C) at 48 h AEL, before the onset of dendrite growth defects in *Rop* mutants, and C4da neuron clones were visualized at 96 h AEL, when dendrite growth defects are broadly manifest in *Rop* mutant C4da neurons. Thus, *shi* was selectively inactivated in these clones from 48 h to 96 h AEL.

Under this temperature regime, we observed a modest decrease in dendrite branching of control neurons (compare Fig. 8E to Fig. 2B), reflecting a mild temperature sensitivity of the branching program,

but little effect on overall dendrite length. *Rop* mutant clones still exhibited characteristic defects, including significant decreases in total dendrite length and an abundance of varicosities along major dendrites (Fig. 8B,E). Blocking *shi* function from 48 h to 96 h AEL reduced overall dendrite growth to a similar extent (Fig. 8C,E), consistent with a previous report that constitutively blocking *shi* function compromises dendrite growth (Yang et al., 2011). In addition, blocking *shi* resulted in a significant increase in dendrite–dendrite crossing events, suggesting that endocytic signaling is required for dendrite–dendrite avoidance (Fig. 8C,G). Interestingly, we found that blocking *shi* function from 48 h to 96 h AEL significantly ameliorated the dendrite defects of *Rop^{G27}* C4da MARCM clones, leading to an overall increase in the number of terminal dendrites and dramatically reducing the appearance of

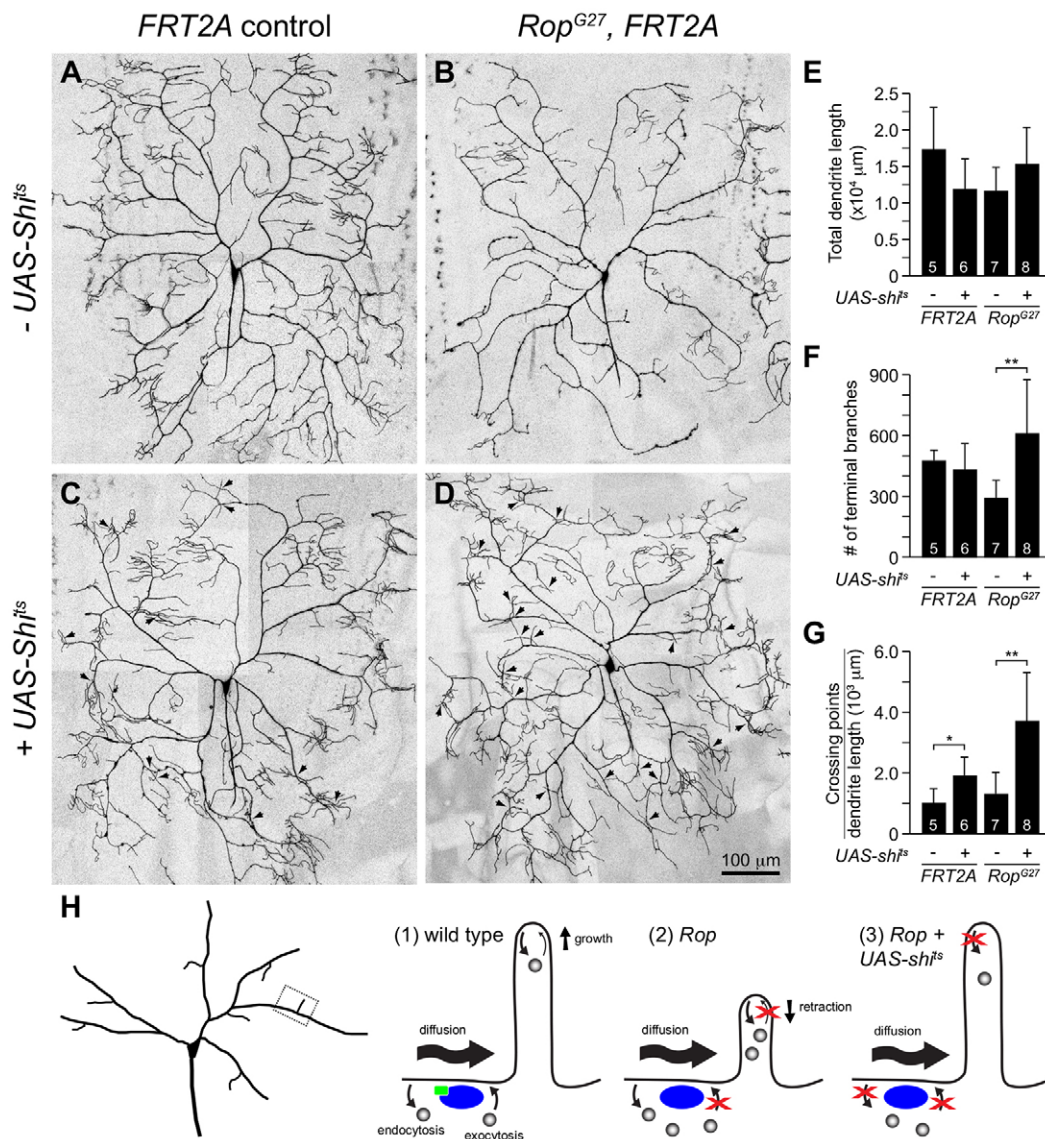


Fig. 8. Blocking endocytosis attenuates dendrite defects in *Rop* mutant neurons. (A–D) Representative images of C4da MARCM clones depicting the effects of blocking endocytosis and exocytosis on dendrite growth. Larvae bearing MARCM clones of the following genotypes are shown: (A) wild-type control; (B) *Rop^{G27}* mutant; (C) C4da neuron expressing UAS-*shi^{ts}*; (D) *Rop^{G27}* mutant C4da neuron expressing UAS-*shi^{ts}* were raised at 25°C for 48 h, shifted to 29°C for 48 h and imaged using live confocal microscopy. Arrows, dendrite–dendrite crossing points. Quantification of the total number of terminal dendrite branches (E), total dendrite length (F) and number of crossing points normalized to dendrite length (G). * $P < 0.05$, ** $P < 0.01$ (Student's *t*-test). The number of neurons analyzed for each genotype is indicated. (H) Model of exocytic and endocytic trafficking in developing dendrites. In wild-type neurons (1), Rop (green rectangle) is recruited to the membrane by the exocyst (blue oval) and mediates exocytosis. In the absence of Rop (2), endocytosis proceeds unchecked causing terminal branch retraction, which can be mitigated by expression of dominant-negative dynamin (3). Means \pm s.d. are shown.

varicosities along the major dendrites (Fig. 8D–F). Thus, endocytosis in the absence of exocytosis is likely to be a major contributor to the terminal dendrite growth defect and degeneration of primary dendrites in *Rop* mutant neurons. We also noted a synergistic effect on dendrite–dendrite crossing defects (Fig. 8D,G), demonstrating that endocytic–exocytic signaling plays crucial roles in dendrite–dendrite avoidance. Altogether, these results demonstrate that the balance of endocytosis and exocytosis is crucial in supporting dendrite growth and maintenance, and that these types of membrane fusion events are differentially localized during neuronal maturation to ensure the correct construction of neuronal architecture.

DISCUSSION

The plasma membrane of the developing neuron must continuously expand to keep pace with the rapid growth of the axon and dendrite. Although the addition of neuronal membrane is mediated by exocytosis, there is little *in vivo* evidence to support the requirement of SM proteins in this process. Our study not only reveals an autonomous function for the SM protein *Rop* and the exocyst in dendrite growth, but also reveals a differential requirement for the exocytosis machinery in the development of different compartments of the dendritic arbor. Depletion of *Rop* in C4da neurons causes an initial defect in terminal dendrites followed by profound degeneration of primary dendrites. Unexpectedly, we found that although *Rop* and the exocyst are required for terminal dendrite growth, *Rop*, the exocyst components *Sec15* and *Sec6*, and *Rop*–*Sec6* complexes are largely excluded from terminal branches. Likewise, we demonstrate that exocytosis predominantly occurs along major dendrites in these neurons, despite the fact that terminal dendrites account for the majority of dendrite growth in larval C4da neurons.

Our results show that terminal dendrites are likely to depend on the diffusion of material from primary dendrites to support their growth and, in the process, reveal key differences in how membrane is allocated in different compartments of the dendritic arbor. Primary and terminal dendrites of C4da neurons differ in their cytoskeletal composition and dynamics (Grueber et al., 2002; Jinushi-Nakao et al., 2007; Lee et al., 2015), which can create differences in membrane tension (Dai and Sheetz, 1999). As membrane tends to flow from a region of low tension to a region of higher tension (Dai and Sheetz, 1995), the resulting tension gradient could then explain how membrane proteins readily diffuse from major branches into terminals, but not in the opposite direction. Why then are terminal dendrites particularly sensitive to reduced *Rop* function? Growing dendrites exhibit high rates of endocytic activity compared to growing axons (Parton et al., 1992; Ye et al., 2007), and dynamic clathrin assembly and disassembly occurs throughout the dendritic arbor, consistent with a requirement for clathrin-dependent endocytosis in dendrite growth (Blanpied et al., 2002; Yang et al., 2011; Zheng et al., 2008). We found that blocking endocytosis significantly ameliorated the terminal dendrite loss observed in *Rop* mutant neurons, suggesting that unchecked endocytosis contributes to the rapid retraction of terminal dendrites in *Rop* mutants. Thus, even though terminal dendrites show low levels of exocytosis compared to primary dendrites, it is necessary to counterbalance the high levels of endocytic activity and replenish the plasma membrane, underscoring the delicate balance of exocytosis and endocytosis that is required for dendrite growth (Fig. 8H).

Although our data suggest that lateral diffusion of material contributes to terminal dendrite growth, we cannot exclude the

possibility that satellite secretory pathways (or Golgi outposts) can act as a local source of membrane within some terminal branches (Horton et al., 2005; Ye et al., 2007). The presence of Golgi outposts within terminal branches of C4da neurons would seem to suggest that local exocytosis is an important mode of terminal dendrite growth, but recent studies support microtubule nucleation as a key role for Golgi outposts within these branches (Ori-McKenney et al., 2012). Therefore, we propose a model in which primary dendrites are the major sites of exocytosis and membrane addition for expansion of the dendritic arbor, and in which terminal dendrites primarily rely on the diffusion of material to support their growth (Fig. 8H).

In mature dendrites, exocytosis primarily occurs in dendritic spines that are enriched with clusters of the target (t)-SNARE syntaxin 4, which mediates activity-dependent exocytosis during long-term potentiation (Kennedy et al., 2010). By contrast, how sites of exocytosis are defined in a growing dendrite remains largely unresolved. The restricted localization of *Rop* in primary dendrites of C4da neurons suggests that the exocytic machinery is likewise targeted to specific sites of membrane expansion during development. Consistent with this notion, *Rop* interacts with exocyst subunits *Sec5* and *Sec6* to regulate dendrite growth, demonstrating that the exocyst–*Sec1* interaction is functionally relevant in higher eukaryotes and could be an important mechanism by which SNARE complexes are recruited to specific sites of membrane expansion. In our BiFC analysis, we found that *Rop* directly interacts with *Sec6* and that these complexes accumulate at sites with high exocytic activity, reflecting the importance of this interaction in biologically relevant contexts. In epithelial cells, we found that *Rop*–*Sec6* complexes accumulate at junctional domains, consistent with the localized recruitment of the exocyst to regions of the epithelial membrane undergoing active exocytosis (Grindstaff et al., 1998), and suggesting that BiFC between *Rop* and *Sec6* can be used as a proxy for exocytic activity in neurons. Indeed, we found that *Rop*–*Sec6* complexes accumulate along major dendritic branches in C4da neurons, which correlate with the primary sites of exocytosis, as revealed by the *in vivo* pH-Tom reporter. Thus, we propose that the exocyst actively recruits *Rop* to specific sites of membrane expansion in dendrites in order to promote growth.

We also observed the accumulation of *Rop*–*Sec6* complexes in C4da axon terminals. This result, together with the axon phenotype that we observed in *Rop* mutant neurons, points to a role for *Rop* in vesicular trafficking in axon growth and/or maintenance, in addition to its well-characterized role in synaptic vesicle release. The exocyst plays a key role in axon outgrowth and discriminates between vesicular trafficking mechanisms that regulate membrane insertion and cell growth, and those that regulate neurotransmitter secretion (Murthy et al., 2003). The exocyst itself is dispensable for neurotransmitter release (Mehta et al., 2005; Murthy et al., 2003), suggesting that binding of *Rop* to the exocyst can differentially affect *Rop*-mediated vesicular trafficking events in the presynaptic terminal.

Our finding that *Rop*^{G27} C4da MARCM clones show a progressive loss of terminal dendrites and blebbing and/or fragmentation of primary dendrites during later stages of larval development further suggests that *Rop* is not only important for growth, but is also broadly required for dendrite maintenance. The neurodegeneration in *Rop* mutant neurons parallels observations in neurons from *munc18-1* knockout mice, which show severe and widespread neurodegeneration (Heeroma et al., 2004; Verhage et al., 2000). Importantly, degeneration in *munc18-1* null neurons cannot be fully explained by the loss of synaptic activity because mice deficient for both *munc13-1* and *munc13-2*, which are

synaptically silent, show no apparent signs of neurodegeneration (Varoqueaux et al., 2002). The function of Munc18-1 in neuronal maintenance is therefore likely to entail a function that is distinct from its role in neurotransmitter secretion. The ability of a dominant-negative allele of *shibire* to mitigate dendrite degeneration phenotypes of *Rop* mutant neurons suggests that a failure in exocytosis of vesicles derived from dynamin-dependent pathways is part of the mechanism by which *Rop* depletion causes degeneration of primary dendrites. Indeed, endocytic dysfunction is a common theme in neurodegeneration and is likely to underlie the pathology of many neurodegenerative disorders (Nixon, 2005). Given the strong association of Munc18-1 with syntaxin-1 (Sudhof and Rothman, 2009), it is not surprising then that a recent study also showed that expression of a dominant-negative form of dynamin could delay neurodegeneration induced by botulinum toxin-mediated cleavage of syntaxin-1 in cultured hippocampal neurons (Peng et al., 2013). Syntaxin-1 is therefore important for neuronal maintenance, but an early requirement for syntaxin-1 in neurite outgrowth (Igarashi et al., 1996) is consistent with the differential requirement for the exocytic machinery in the developing neuron.

Our findings are particularly interesting in light of the fact that mutations in *MUNC18-1* and exocyst subunit genes are associated with a spectrum of neurodevelopmental disorders. *De novo* mutations in the gene encoding MUNC18-1 have been identified in individuals diagnosed with Ohtahara syndrome (Saito et al., 2008). In addition to intractable seizures, individuals with mutations in *MUNC18-1* further exhibit profound intellectual disability, physical deficits and varying degrees of cerebral atrophy (Saito et al., 2008). Although disruption of *MUNC18-1* is most closely associated with Ohtahara syndrome, *de novo* mutations in *MUNC18-1* have also been identified in individuals with severe intellectual disability and non-syndromic epilepsy, individuals with non-syndromic intellectual disability, and individuals with Rett syndrome (Hamdan et al., 2011, 2009; Olson et al., 2015; Romaniello et al., 2015). Likewise, recent studies have revealed possible connections between mutations in exocyst genes and neurological disorders (Evers et al., 2014; Fröhmes et al., 2013; Wen et al., 2013). Given that dendrite defects are the strongest pathological correlate of intellectual disability (Kaufmann and Moser, 2000), we speculate that dendritic abnormalities might contribute to intellectual disability that is associated with *MUNC18-1* and exocyst dysfunction.

MATERIALS AND METHODS

Fly stocks

The following lines were used: *Gal4²²¹* (Grueber et al., 2003), *ppk-Gal4* (Grueber et al., 2007), *A58-Gal4* (Galko and Krasnow, 2004), *ppk-Frt-stop-Frt-Gal4* (Kanamori et al., 2013), *UAS-pHluorin-CD4-tdTomato* (Kanamori et al., 2015), *E7-2-36* (Brewster and Bodmer, 1995), *SOP-FLP* (Shimono et al., 2014), *UAS-myrEos* (Pfeiffer et al., 2010), *ppk-CD4-tdTomato*, *UAS-CD4-tdGFP* and *UAS-CD4-tdTomato* (Han et al., 2011), *UAS-shi.K44A* (Moline et al., 1999), and *UAS-Dicer-2* (Dietz et al., 2007). *Rop^{G27}* and *Rop^{A19}* (Harrison et al., 1994), *Sec5^{E10}* and *Sec5^{E13}* (Murthy et al., 2003), *Sec6^{Ex15}* (Murthy et al., 2005), *Sec6^{A20}* (Beronja et al., 2005), and *UAS-GFP::Sec15* (Jafar-Nejad et al., 2005) have been described previously. RNAi lines were generated by the Transgenic RNAi Project at Harvard Medical School (Ni et al., 2009). *UAS-NYFP-Rop* and *UAS-CYFP-Sec6* transgenic lines were generated by site-specific integration into *attP40* and *attP2* docker lines, respectively.

MARCM labeling

Rop^{G27}, *FRT2A/TM6B*, *Rop^{A19}*, *FRT2A/TM6B* or *w*; *FRT2A* were mated with *109(2)80-Gal4*, *UAS-mCD8::GFP*, *SOP-FLP*; *tub-Gal80*, *FRT4A*

females. *Sec5^{E10}*, *FRT40A/CyO* or *w*; *FRT40A* males were mated with *elav-Gal4*, *UAS-mCD8::GFP*, *hsFLP*; *tub-Gal80*, *FRT40A* females, and *FRT42D*, *Sec6^{Ex15}/CyO* or *w*; *FRT42D* males were mated with *elav-Gal4*, *UAS-mCD8::GFP*, *hsFLP*; *FRT42D*, *tub-Gal80* females. For *SOP-FLP*-bearing crosses, embryos were collected for 2 h in standard cornmeal molasses agar and allowed to develop for 72, 96 or 144 h, at which time MARCM clones were imaged live using confocal microscopy. For *hsFLP*-bearing crosses, embryos were collected for 2 h on grape juice agar plates and allowed to develop for 3 to 5 h at 25°C before being heat-shocked for 1 h at 38°C. Embryos were then allowed to develop to late third instar larvae, at which point they were dissected and processed for immunocytochemistry.

Immunocytochemistry

Embryos and larvae were processed for immunocytochemistry, as previously described (Kim et al., 2006), using the following antibodies: mouse anti-Rop 4F8 at 1:200 (Developmental Studies Hybridoma Bank) (Harrison et al., 1994), rabbit anti-Myc at 1:1000 (A-14, Santa Cruz Biotechnology), rabbit anti-β-galactosidase at 1:5000 (Cortex Biochem), rat anti-mCD8 at 1:200 (Life Technologies), rabbit anti-Dcp-1 at 1:500 (Cell Signaling Technologies), Cy5-conjugated anti-horseradish-peroxidase at 1:250 (Jackson Laboratories), and appropriate fluorophore-conjugated secondary antibodies at 1:200 (Jackson Laboratories). Whole-mount embryos and image stacks of MARCM clones were acquired at 1024×1024-pixel resolution using either a Leica TCS SP2 or an Olympus FluoView FV1000 confocal microscope.

Live imaging

At the appropriate time, a single embryo or larva was mounted in 90% glycerol and imaged on a Leica SP5 confocal microscope with a 40×1.25NA lens. MARCM clones were imaged at 1024×1024-pixel resolution. For late time points, image stacks from multiple fields of view were assembled into a montage. For pHluorin imaging, larvae of the genotype *ppk-gal4/UAS-pHluorin::CD4-tdTomato* were imaged at 96 h AEL, and larvae of the genotype *UAS-hsFLP/+; ppk-Frt-stop-Frt-Gal4/UAS-pHluorin::CD4-tdTomato; UAS-pHluorin::CD4-tdTomato/+* were heat shocked (37°C for 1 h) at 48 h AEL and imaged at 72 h AEL at 1024×512-pixel resolution. For BiFC imaging, larvae of the genotype *ppk-Gal4/UAS-NYFP::Rop; ppk-CD4tdTomato/UAS-Sec6::CYFP* were imaged at 96 h AEL at 1024×512-pixel resolution.

FRAP analysis of membrane protein diffusion

Photoconversion and FRAP assays were conducted on a Leica SP5 with a 40×1.25NA oil objective at 1024×256-pixel resolution. For photoconversion assays, 10 μm of either a terminal or a major dendrite of a *ppk-gal4/+; UAS-myr-tdEosFP/+* or *ppk-gal4/+; UAS-tdEosFP/+* larva at 72 h AEL was selected as a region of interest (ROI). The ROI was illuminated for 5 s with a 50-mW 405-nm Diode laser (Leica) at 40% output to photoconvert tdEos and imaged at 10 s and 300 s post-conversion with a 500–520-nm bandwidth. The fluorescence intensity of the converted signal was measured for the central 8 μm of the converted region and the adjacent 8 μm in both directions. Intensity was analyzed using line plots (ImageJ) with eight individual samples. For FRAP assays, ROIs in control and *Rop^{G27}* mutant C4da MARCM clones were photobleached for 3 s with a 405-nm laser at 60% power such that 50% of the initial fluorescence intensity was bleached. Baseline fluorescence was measured from five images acquired before bleaching, and fluorescence recovery was measured with 20 scans at 2-s intervals after bleaching. Background fluorescence values were subtracted from measurements of a nearby unbleached dendritic region at each time point. To control for photobleaching and sample movement out of focus, fluorescence intensity was monitored in multiple regions of the arbor outside of the ROI; only samples for which intensities remained steady in these control regions were included in data analysis. Recovery half-time and the recoverable pool were measured using Leica FRAP Wizard software.

Immunoprecipitation

Adult fly heads (50 per experiment) were isolated and homogenized in 500 ml of lysis buffer (15 mM Tris-HCl at pH 7.6, 0.25 mM sucrose, 15 mM

NaCl, 15 mM MgCl₂, 25 mM EDTA, 1 mM EGTA and protease inhibitor cocktail). After pre-clearing with Protein-A agarose (Life Technologies), extracts were incubated with 15 ml of anti-Rop antibody and 50 ml of Protein-A agarose beads. The beads and input extract were eluted 1:1 in Laemmli buffer with 2-mercaptoethanol (Bio-Rad Laboratories) and boiled for 5 min. Samples were resolved on a 4–20% polyacrylamide gel and transferred to a nitrocellulose membrane. Membranes were blocked for 1 h in Blocking Buffer (Rockland Immunochemicals) and incubated overnight at 4°C with primary antibodies against Sec6 at 1:250 (Beronja et al., 2005) or against Sec15 at 1:250 (Mehta et al., 2005). Membranes were then incubated with secondary antibodies (anti-guinea pig IRDye700 at 1:10,000; Rockland Immunochemicals), and blots were imaged and processed on an Odyssey Infrared Imaging System (LI-COR Biosciences).

Bimolecular fluorescence complementation

Rop and *Sec6* coding sequences were PCR amplified from genomic DNA and inserted into *pUAST-BiFC* vectors (Gohl et al., 2010) using Gateway cloning (Life Technologies) to generate expression vectors with *Rop* fused to coding sequences for the N-terminal portion of YFP and *Sec6* fused to the C-terminal portion of YFP (*pUAST-NYFP-Rop*, *pUAST-Rop-NYFP*, *pUAST-CYFP-Sec6*, *pUAST-Sec6-CYFP*). As negative controls, we generated *pUAST-NYFP* and *pUAST-CYFP* expression vectors that contained coding sequences for the N-terminal and C-terminal portion of YFP, respectively. To assay for YFP reconstitution, we used Effectene (Qiagen) to transfect S2 cells with *Actin-Gal4*, *UAS-RFP* and all possible combinations of the above *NYFP* and *CYFP* expression constructs; only *pUAST-NYFP-Rop+pUAST-Sec6-CYFP* yielded a signal upon BiFC analysis, therefore we used those expression constructs to monitor Rop–Sec6 complex formation *in vivo*.

Quantitative and statistical analysis

Two-dimensional projections of image z-stacks were used for computer-assisted dendrite tracing and analysis with either the NeuronJ plugin in ImageJ (Meijering et al., 2004) or Neurolucida (Figs 2, 4 and 8; MBF Bioscience). For Sholl analysis (Sholl, 1953), neuron traces were generated in NeuronJ, and analysis was performed using the Sholl Analysis plugin in ImageJ. Statistical tests are indicated in the figure legends.

Acknowledgements

We thank Hugo Bellen, Thomas Schwarz, Ulrich Tepass, Kazuo Emoto, the Bloomington Stock Center, and the Developmental Studies Hybridoma Bank for fly stocks and antibodies; Sven Bogdan for BiFC vectors; and Kazuo Emoto, Peter Soba, Daichi Kamiyama and Mark Eddison for critical reading of the manuscript.

Competing interests

The authors declare no competing or financial interests.

Author contributions

J.Z.P. and M.D.K. designed the research; Y.P., J.L., K.R., Y.H., N.C., S.L., J.Z.P. and M.D.K. performed research; Y.P., J.L., K.R., H.H., S.L., J.Z.P. and M.D.K. analyzed data; J.Z.P. and M.D.K. wrote the paper.

Funding

This work was supported by National Institutes of Health (NIH) [grant numbers R21-NS072588 to M.D.K., R00-MH084277 and R01-NS076614 to J.Z.P.]; the Stanley J. Glaser Foundation (to M.D.K.); a March of Dimes Basil O'Connor Starter Scholar Award; and a Klingenstein Fellowship in Neuroscience (to J.Z.P.). Deposited in PMC for release after 12 months.

Supplementary information

Supplementary information available online at <http://jcs.biologists.org/lookup/suppl/doi:10.1242/jcs.174771/-/DC1>

References

- Beronja, S., Laprise, P., Papoulas, O., Pelikka, M., Sisson, J. and Tepass, U. (2005). Essential function of *Drosophila* Sec6 in apical exocytosis of epithelial photoreceptor cells. *J. Cell Biol.* **169**, 635–646.
- Blanpied, T. A., Scott, D. B. and Ehlers, M. D. (2002). Dynamics and regulation of clathrin coats at specialized endocytic zones of dendrites and spines. *Neuron* **36**, 435–449.
- Bray, D. (1970). Surface movements during the growth of single explanted neurons. *Proc. Natl. Acad. Sci. USA* **65**, 905–910.
- Brewster, R. and Bodmer, R. (1995). Origin and specification of type II sensory neurons in *Drosophila*. *Development* **121**, 2923–2936.
- Carr, C. M., Grote, E., Munson, M., Hughson, F. M. and Novick, P. J. (1999). Sec1p binds to SNARE complexes and concentrates at sites of secretion. *J. Cell Biol.* **146**, 333–344.
- Craig, A. M., Wyborski, R. J. and Banker, G. (1995). Preferential addition of newly synthesized membrane protein at axonal growth cones. *Nature* **375**, 592–594.
- Dai, J. and Sheetz, M. P. (1995). Axon membrane flows from the growth cone to the cell body. *Cell* **83**, 693–701.
- Dai, J. and Sheetz, M. P. (1999). Membrane tether formation from blebbing cells. *Biophys. J.* **77**, 3363–3370.
- Dietzl, G., Chen, D., Schnorrer, F., Su, K.-C., Barinova, Y., Fellner, M., Gasser, B., Kinsey, K., Oppel, S., Scheiblaue, S. et al. (2007). A genome-wide transgenic RNAi library for conditional gene inactivation in *Drosophila*. *Nature* **448**, 151–156.
- Evers, C., Maas, B., Koch, K. A., Jauch, A., Janssen, J. W. G., Sutter, C., Parker, M. J., Hinderhofer, K. and Moog, U. (2014). Mosaic deletion of *EXOC6B*: further evidence for an important role of the exocyst complex in the pathogenesis of intellectual disability. *Am. J. Med. Genet. A* **164**, 3088–3094.
- Foley, E. and O'Farrell, P. H. (2004). Functional dissection of an innate immune response by a genome-wide RNAi screen. *PLoS Biol.* **2**, e203.
- Frühmesser, A., Blake, J., Haberlandt, E., Baying, B., Raeder, B., Runz, H., Spreiz, A., Fauth, C., Benes, V., Utermann, G. et al. (2013). Disruption of *EXOC6B* in a patient with developmental delay, epilepsy, and a *de novo* balanced t(2;8) translocation. *Eur. J. Hum. Genet.* **21**, 1177–1180.
- Galko, M. J. and Krasnow, M. A. (2004). Cellular and genetic analysis of wound healing in *Drosophila* larvae. *PLoS Biol.* **2**, e239.
- Garcia, E. P., McPherson, P. S., Chilcote, T. J., Takei, K. and De Camilli, P. (1995). rSec1A and B colocalize with syntaxin 1 and SNAP-25 throughout the axon, but are not in a stable complex with syntaxin. *J. Cell Biol.* **129**, 105–120.
- Gohl, C., Banovic, D., Grevelhorster, A. and Bogdan, S. (2010). WAVE forms hetero- and homo-oligomeric complexes at integrin junctions in *Drosophila* visualized by bimolecular fluorescence complementation. *J. Biol. Chem.* **285**, 40171–40179.
- Grindstaff, K. K., Yeaman, C., Anandasabapathy, N., Hsu, S.-C., Rodriguez-Boulant, E., Scheller, R. H. and Nelson, W. J. (1998). Sec6/8 complex is recruited to cell–cell contacts and specifies transport vesicle delivery to the basal-lateral membrane in epithelial cells. *Cell* **93**, 731–740.
- Grote, E., Carr, C. M. and Novick, P. J. (2000). Ordering the final events in yeast exocytosis. *J. Cell Biol.* **151**, 439–452.
- Grueber, W. B., Jan, L. Y. and Jan, Y. N. (2002). Tiling of the *Drosophila* epidermis by multidendritic sensory neurons. *Development* **129**, 2867–2878.
- Grueber, W. B., Jan, L. Y. and Jan, Y. N. (2003). Different levels of the homeodomain protein Cut regulate distinct dendrite branching patterns of *Drosophila* multidendritic neurons. *Cell* **112**, 805–818.
- Grueber, W. B., Ye, B., Yang, C.-H., Younger, S., Borden, K., Jan, L. Y. and Jan, Y.-N. (2007). Projections of *Drosophila* multidendritic neurons in the central nervous system: links with peripheral dendrite morphology. *Development* **134**, 55–64.
- Hamdan, F. F., Piton, A., Gauthier, J., Lortie, A., Dubeau, F., Dobrzaniecka, S., Spiegelman, D., Noreau, A., Pellerin, S., Côté, M. et al. (2009). De novo *STXBP1* mutations in mental retardation and nonsyndromic epilepsy. *Ann. Neurol.* **65**, 748–753.
- Hamdan, F. F., Gauthier, J., Dobrzaniecka, S., Lortie, A., Mottion, L., Vanasse, M., D'Anjou, G., Lacaille, J. C., Rouleau, G. A. and Michaud, J. L. (2011). Intellectual disability without epilepsy associated with *STXBP1* disruption. *Eur. J. Hum. Genet.* **19**, 607–609.
- Han, C., Jan, L. Y. and Jan, Y.-N. (2011). Enhancer-driven membrane markers for analysis of nonautonomous mechanisms reveal neuron–glia interactions in *Drosophila*. *Proc. Natl. Acad. Sci. USA* **108**, 9673–9678.
- Harrison, S. D., Broadie, K., van de Goor, J. and Rubin, G. M. (1994). Mutations in the *Drosophila* *Rop* gene suggest a function in general secretion and synaptic transmission. *Neuron* **13**, 555–566.
- Hata, Y., Slaughter, C. A. and Südhof, T. C. (1993). Synaptic vesicle fusion complex contains *unc-18* homologue bound to syntaxin. *Nature* **366**, 347–351.
- Hazuka, C. D., Foletti, D. L., Hsu, S. C., Kee, Y., Hopf, F. W. and Scheller, R. H. (1999). The sec6/8 complex is located at neurite outgrowth and axonal synapse-assembly domains. *J. Neurosci.* **19**, 1324–1334.
- Heeroma, J. H., Roelandse, M., Wierda, K., van Aerde, K. I., Toonen, R. F. G., Hensbroek, R. A., Brussaard, A., Matus, A. and Verhage, M. (2004). Trophic support delays but does not prevent cell-intrinsic degeneration of neurons deficient for munc18-1. *Eur. J. Neurosci.* **20**, 623–634.
- Horton, A. C., Rácz, B., Monson, E. E., Lin, A. L., Weinberg, R. J. and Ehlers, M. D. (2005). Polarized secretory trafficking directs cargo for asymmetric dendrite growth and morphogenesis. *Neuron* **48**, 757–771.
- Hu, C.-D., Chinenov, Y. and Kerppola, T. K. (2002). Visualization of interactions among bZIP and Rel family proteins in living cells using bimolecular fluorescence complementation. *Mol. Cell* **9**, 789–798.

- Igarashi, M., Kozaki, S., Terakawa, S., Kawano, S., Ide, C. and Komiya, Y. (1996). Growth cone collapse and inhibition of neurite growth by Botulinum neurotoxin C1: a t-SNARE is involved in axonal growth. *J. Cell Biol.* **134**, 205–215.
- Jafar-Nejad, H., Andrews, H. K., Acar, M., Bayat, V., Wirtz-Peitz, F., Mehta, S. Q., Knoblich, J. A. and Bellen, H. J. (2005). Sec15, a component of the exocyst, promotes notch signaling during the asymmetric division of *Drosophila* sensory organ precursors. *Dev. Cell* **9**, 351–363.
- Jiang, N., Soba, P., Parker, E., Kim, C. C. and Parrish, J. Z. (2014). The microRNA *bantam* regulates a developmental transition in epithelial cells that restricts sensory dendrite growth. *Development* **141**, 2657–2668.
- Jinushi-Nakao, S., Arvind, R., Amikura, R., Kinameri, E., Liu, A. W. and Moore, A. W. (2007). Knot/Collier and Cut control different aspects of dendrite cytoskeleton and synergize to define final arbor shape. *Neuron* **56**, 963–978.
- Kanamori, T., Kanai, M. I., Dairyo, Y., Yasunaga, K.-i., Morikawa, R. K. and Emoto, K. (2013). Compartmentalized calcium transients trigger dendrite pruning in *Drosophila* sensory neurons. *Science* **340**, 1475–1478.
- Kanamori, T., Yoshino, J., Yasunaga, K.-i., Dairyo, Y. and Emoto, K. (2015). Local endocytosis triggers dendritic thinning and pruning in *Drosophila* sensory neurons. *Nat. Commun.* **6**, 6515.
- Kaufmann, W. E. and Moser, H. W. (2000). Dendritic anomalies in disorders associated with mental retardation. *Cereb. Cortex* **10**, 981–991.
- Kennedy, M. J., Davison, I. G., Robinson, C. G. and Ehlers, M. D. (2010). Syntaxin-4 defines a domain for activity-dependent exocytosis in dendritic spines. *Cell* **141**, 524–535.
- Kim, M. D., Jan, L. Y. and Jan, Y. N. (2006). The bHLH-PAS protein Spineless is necessary for the diversification of dendrite morphology of *Drosophila* dendritic arborization neurons. *Genes Dev.* **20**, 2806–2819.
- Kitamoto, T. (2001). Conditional modification of behavior in *Drosophila* by targeted expression of a temperature-sensitive *shibire* allele in defined neurons. *J. Neurobiol.* **47**, 81–92.
- Lalli, G. and Hall, A. (2005). Ral GTPases regulate neurite branching through GAP-43 and the exocyst complex. *J. Cell Biol.* **171**, 857–869.
- Lee, T. and Luo, L. (1999). Mosaic analysis with a repressible cell marker for studies of gene function in neuronal morphogenesis. *Neuron* **22**, 451–461.
- Lee, J., Peng, Y., Lin, W.-Y. and Parrish, J. Z. (2015). Coordinate control of terminal dendrite patterning and dynamics by the membrane protein Raw. *Development* **142**, 162–173.
- Lockerbie, R. O., Miller, V. E. and Pfenninger, K. H. (1991). Regulated plasmalemmal expansion in nerve growth cones. *J. Cell Biol.* **112**, 1215–1227.
- Mehta, S. Q., Hiesinger, P. R., Beronja, S., Zhai, R. G., Schulze, K. L., Verstreken, P., Cao, Y., Zhou, Y., Tepass, U., Crair, M. C. et al. (2005). Mutations in *Drosophila* *sec15* reveal a function in neuronal targeting for a subset of exocyst components. *Neuron* **46**, 219–232.
- Meijering, E., Jacob, M., Sarria, J.-C. F., Steiner, P., Hirling, H. and Unser, M. (2004). Design and validation of a tool for neurite tracing and analysis in fluorescence microscopy images. *Cytometry* **58A**, 167–176.
- Miesenböck, G., De Angelis, D. A. and Rothman, J. E. (1998). Visualizing secretion and synaptic transmission with pH-sensitive green fluorescent proteins. *Nature* **394**, 192–195.
- Moline, M. M., Southern, C. and Bejsovec, A. (1999). Directionality of wingless protein transport influences epidermal patterning in the *Drosophila* embryo. *Development* **126**, 4375–4384.
- Morgera, F., Sallah, M. R., Dubuke, M. L., Gandhi, P., Brewer, D. N., Carr, C. M. and Munson, M. (2012). Regulation of exocytosis by the exocyst subunit Sec6 and the SM protein Sec1. *Mol. Biol. Cell* **23**, 337–346.
- Murthy, M., Garza, D., Scheller, R. H. and Schwarz, T. L. (2003). Mutations in the exocyst component Sec5 disrupt neuronal membrane traffic, but neurotransmitter release persists. *Neuron* **37**, 433–447.
- Murthy, M., Ranjan, R., Deneff, N., Higashi, M. E. L., Schupbach, T. and Schwarz, T. L. (2005). Sec6 mutations and the *Drosophila* exocyst complex. *J. Cell Sci.* **118**, 1139–1150.
- Ni, J.-Q., Liu, L.-P., Binari, R., Hardy, R., Shim, H.-S., Cavallaro, A., Booker, M., Pfeiffer, B. D., Markstein, M., Wang, H. et al. (2009). A *Drosophila* resource of transgenic RNAi lines for neurogenetics. *Genetics* **182**, 1089–1100.
- Nixon, R. A. (2005). Endosome function and dysfunction in Alzheimer's disease and other neurodegenerative diseases. *Neurobiol. Aging* **26**, 373–382.
- Novick, P., Field, C. and Schekman, R. (1980). Identification of 23 complementation groups required for post-translational events in the yeast secretory pathway. *Cell* **21**, 205–215.
- Olson, H. E., Tambunan, D., LaCoursiere, C., Goldenberg, M., Pinsky, R., Martin, E., Ho, E., Khwaja, O., Kaufmann, W. E. and Poduri, A. (2015). Mutations in epilepsy and intellectual disability genes in patients with features of Rett syndrome. *Am. J. Med. Genet. A* **167**, 2017–2025.
- Ori-McKenney, K. M., Jan, L. Y. and Jan, Y.-N. (2012). Golgi outposts shape dendrite morphology by functioning as sites of centrosomal microtubule nucleation in neurons. *Neuron* **76**, 921–930.
- Parrish, J. Z., Kim, M. D., Jan, L. Y. and Jan, Y. N. (2006). Genome-wide analyses identify transcription factors required for proper morphogenesis of *Drosophila* sensory neuron dendrites. *Genes Dev.* **20**, 820–835.
- Parrish, J. Z., Emoto, K., Jan, L. Y. and Jan, Y. N. (2007). Polycomb genes interact with the tumor suppressor genes *hippo* and *warts* in the maintenance of *Drosophila* sensory neuron dendrites. *Genes Dev.* **21**, 956–972.
- Parrish, J. Z., Xu, P., Kim, C. C., Jan, L. Y. and Jan, Y. N. (2009). The microRNA *bantam* functions in epithelial cells to regulate scaling growth of dendrite arbors in *Drosophila* sensory neurons. *Neuron* **63**, 788–802.
- Parton, R. G., Simons, K. and Dotti, C. G. (1992). Axonal and dendritic endocytic pathways in cultured neurons. *J. Cell Biol.* **119**, 123–137.
- Peng, L., Liu, H., Ruan, H., Tepp, W. H., Stoothoff, W. H., Brown, R. H., Johnson, E. A., Yao, W.-D., Zhang, S.-C. and Dong, M. (2013). Cytotoxicity of botulinum neurotoxins reveals a direct role of syntaxin 1 and SNAP-25 in neuron survival. *Nat. Commun.* **4**, 1472.
- Pfeiffer, B. D., Ngo, T.-T. B., Hibbard, K. L., Murphy, C., Jenett, A., Truman, J. W. and Rubin, G. M. (2010). Refinement of tools for targeted gene expression in *Drosophila*. *Genetics* **186**, 735–755.
- Pfenninger, K. H. (2009). Plasma membrane expansion: a neuron's Herculean task. *Nat. Rev. Neurosci.* **10**, 251–261.
- Pfenninger, K. H. and Johnson, M. P. (1983). Membrane biogenesis in the sprouting neuron. I. Selective transfer of newly synthesized phospholipid into the growing neurite. *J. Cell Biol.* **97**, 1038–1042.
- Romaniello, R., Saettini, F., Panzeri, E., Arrigoni, F., Bassi, M. T. and Borgatti, R. (2015). A *de-novo* STXBP1 gene mutation in a patient showing the Rett syndrome phenotype. *Neuroreport* **26**, 254–257.
- Saito, H., Kato, M., Mizuguchi, T., Hamada, K., Osaka, H., Tohyama, J., Urano, K., Kumada, S., Nishiyama, K., Nishimura, A. et al. (2008). *De novo* mutations in the gene encoding STXBP1 (MUNC18-1) cause early infantile epileptic encephalopathy. *Nat. Genet.* **40**, 782–788.
- Shimono, K., Fujishima, K., Nomura, T., Ohashi, M., Usui, T., Kengaku, M., Toyoda, A. and Uemura, T. (2014). An evolutionarily conserved protein CHORD regulates scaling of dendritic arbors with body size. *Sci. Rep.* **4**, 4415.
- Sholl, D. A. (1953). Dendritic organization in the neurons of the visual and motor cortices of the cat. *J. Anat.* **87**, 387–406.
- Sudhof, T. C. and Rothman, J. E. (2009). Membrane fusion: grappling with SNARE and SM proteins. *Science* **323**, 474–477.
- TerBush, D. R., Maurice, T., Roth, D. and Novick, P. (1996). The Exocyst is a multiprotein complex required for exocytosis in *Saccharomyces cerevisiae*. *EMBO J.* **15**, 6483–6494.
- Varoqueaux, F., Sigler, A., Rhee, J.-S., Brose, N., Enk, C., Reim, K. and Rosenmund, C. (2002). Total arrest of spontaneous and evoked synaptic transmission but normal synaptogenesis in the absence of Munc13-mediated vesicle priming. *Proc. Natl. Acad. Sci. USA* **99**, 9037–9042.
- Vega, I. E. and Hsu, S. C. (2001). The exocyst complex associates with microtubules to mediate vesicle targeting and neurite outgrowth. *J. Neurosci.* **21**, 3839–3848.
- Verhage, M., Maia, A. S., Plomp, J. J., Brussaard, A. B., Heeroma, J. H., Vermeer, H., Toonen, R. F., Hammer, R. E., van den Berg, T. K., Missler, M. et al. (2000). Synaptic assembly of the brain in the absence of neurotransmitter secretion. *Science* **287**, 864–869.
- Wen, J., Lopes, F., Soares, G., Farrell, S. A., Nelson, C., Qiao, Y., Martell, S., Badukke, C., Bessa, C., Ylstra, B. et al. (2013). Phenotypic and functional consequences of haploinsufficiency of genes from exocyst and retinoic acid pathway due to a recurrent microdeletion of 2p13.2. *Orphanet J. Rare Dis.* **8**, 100.
- Wiederkehr, A., De Craene, J.-O., Ferro-Novick, S. and Novick, P. (2004). Functional specialization within a vesicle tethering complex: bypass of a subset of exocyst deletion mutants by Sec1p or Sec4p. *J. Cell Biol.* **167**, 875–887.
- Yang, W.-K., Peng, Y.-H., Li, H., Lin, H.-C., Lin, Y.-C., Lai, T.-T., Suo, H., Wang, C.-H., Lin, W.-H., Ou, C. Y. et al. (2011). Nak regulates localization of clathrin sites in higher-order dendrites to promote local dendrite growth. *Neuron* **72**, 285–299.
- Ye, B., Zhang, Y., Song, W., Younger, S. H., Jan, L. Y. and Jan, Y. N. (2007). Growing dendrites and axons differ in their reliance on the secretory pathway. *Cell* **130**, 717–729.
- Zheng, J., Shen, W.-H., Lu, T.-J., Zhou, Y., Chen, Q., Wang, Z., Xiang, T., Zhu, Y.-C., Zhang, C., Duan, S. et al. (2008). Clathrin-dependent endocytosis is required for TrkB-dependent Akt-mediated neuronal protection and dendritic growth. *J. Biol. Chem.* **283**, 13280–13288.

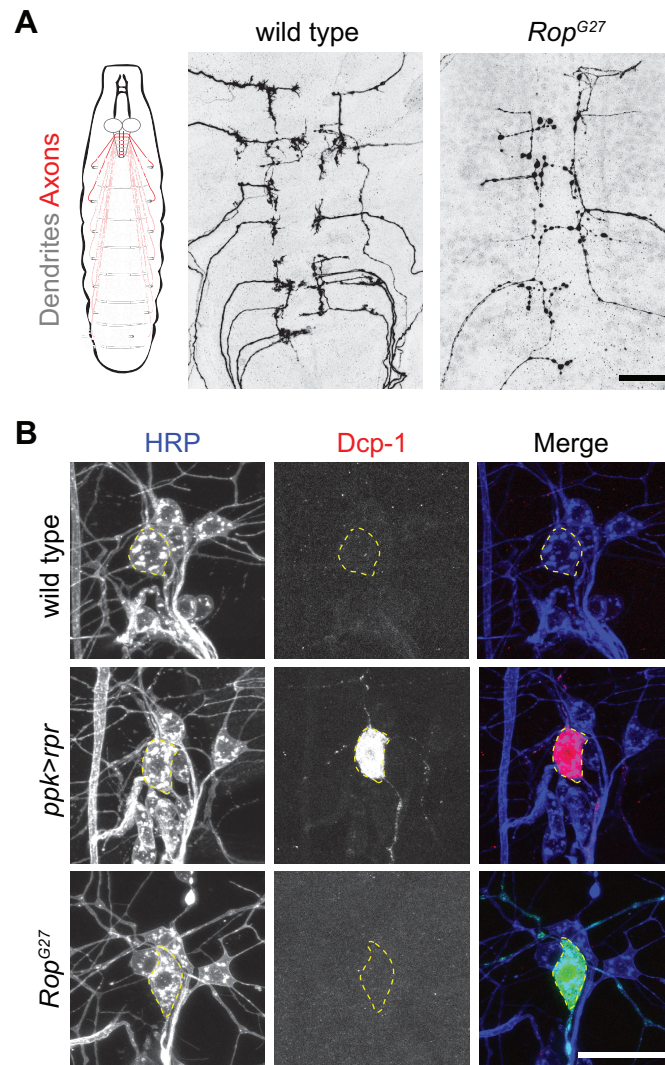


Figure S1. Axon and dendrite phenotypes of *Rop* mutant neurons are unlikely to be a consequence of cell death. (A) Axons of *Rop*^{G27} da neuron MARCM clones appear thin with varicosities along the terminals at 144 h AEL compared to wild-type controls. (B) Dorsal cluster of da neurons as revealed by staining with horseradish peroxidase (HRP). Wild-type C4da neurons and *Rop*^{G27} C4da-ddaC MARCM clones (labeled in green) show no detectable signal for Death caspase-1 (Dcp-1). By contrast, C4da neurons expressing the apoptosis activator Reaper (*ppk>rpr*) stain positive for Dcp-1. Scale bars, 25 μm.

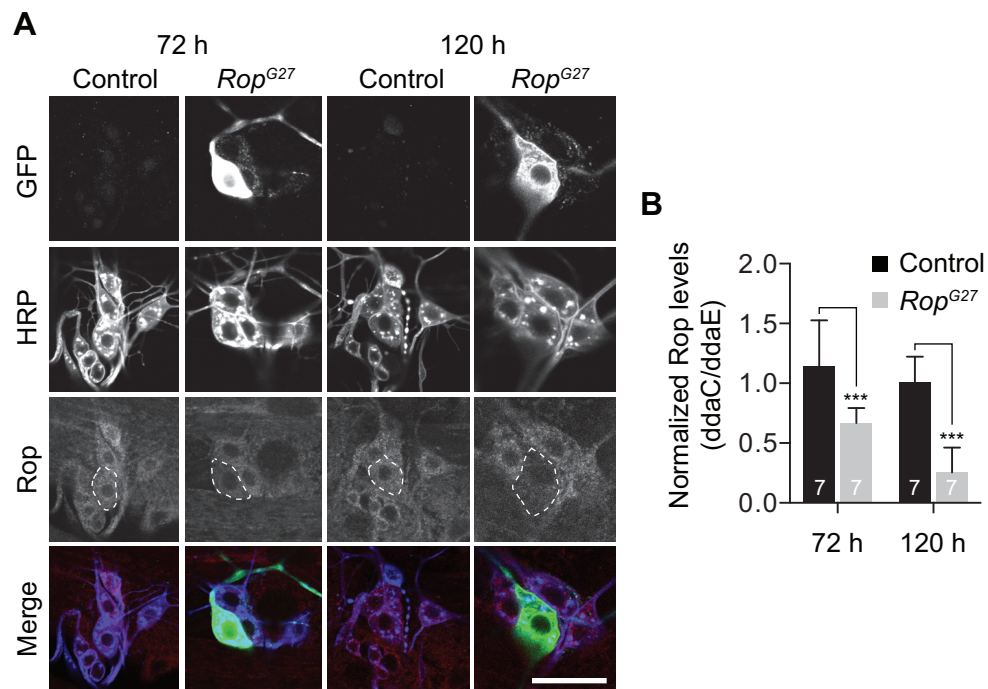


Figure S2. Rop protein perdures through early larval stages in *Rop^{G27}* mutant C4da MARCM clones. (A) *Rop^{G27}* mutant C4da MARCM clones and *Rop^{G27/+}* heterozygous control C4da neurons (from the neighboring segment in the same larva) were stained with antibodies for HRP (to label sensory neurons) and Rop. Representative images and (B) quantification (mean and standard deviation, number of neurons indicated for each sample) of Rop levels (mean Rop immunoreactivity in the C4da soma, outlined with white hatched line) are shown for each genotype-timepoint combination. Scale bar, 25 μ m.

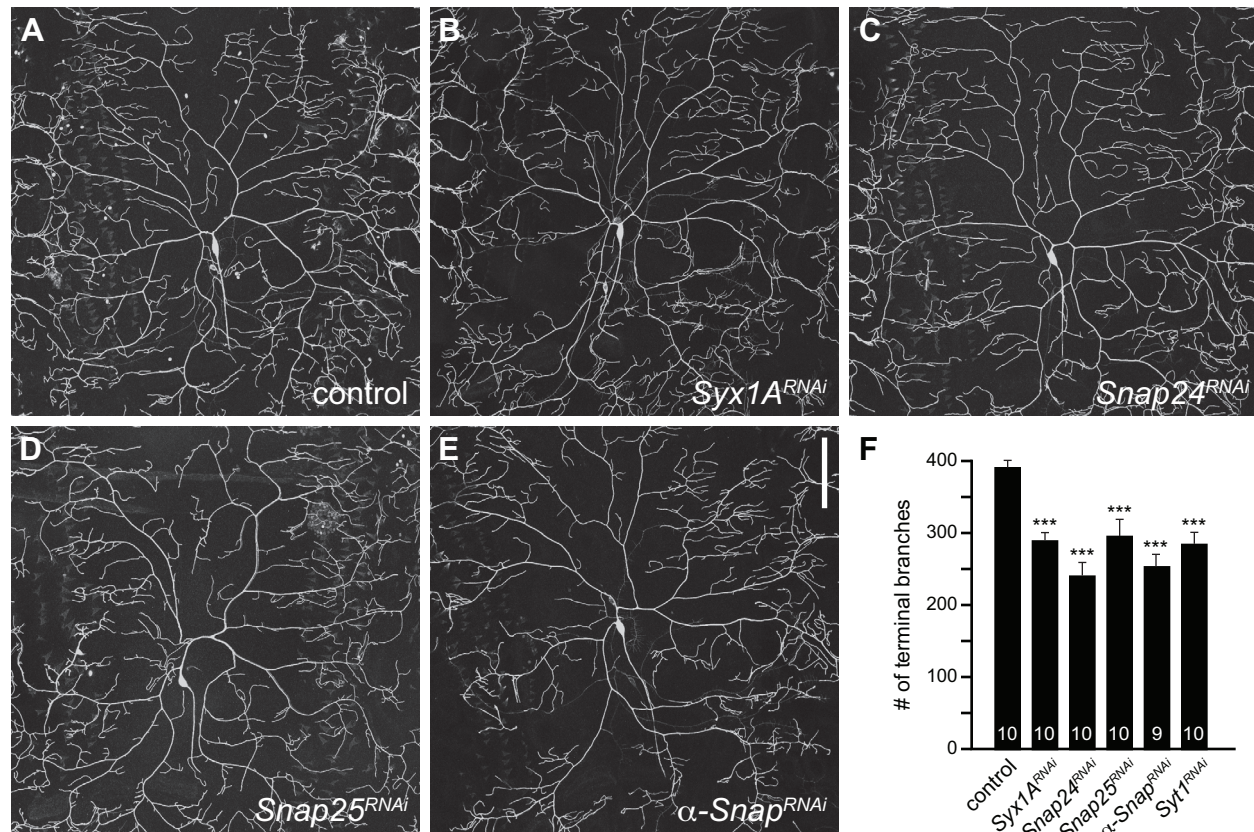


Figure S3. SNARE proteins regulate terminal dendritic branching. Dendritic morphologies of representative C4da neurons in a *UAS-Dicer-2* control (A) or expressing RNAi transgenes targeting *Syx1A* (B), *Snap24* (C), *Snap25* (D), and *α-Snap* (E). (F) Mean and standard deviation of terminal branch number with the number of neurons analyzed for each genotype indicated. *** $p < 0.001$, compared to control (one-way ANOVA with Tukey's HSD *post hoc* analysis). Scale bar, 50 μ m.

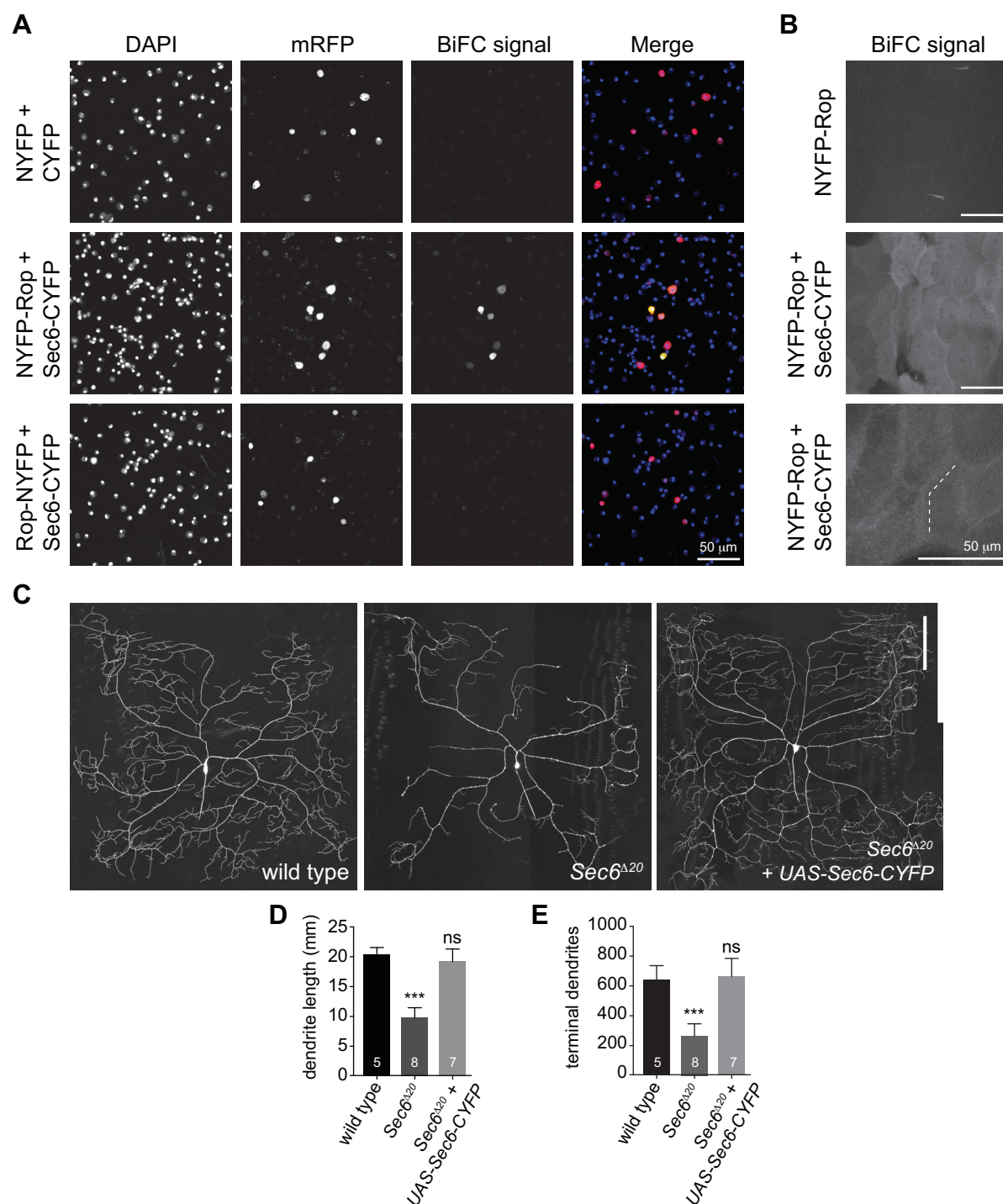


Figure S4. Monitoring Rop-Sec6 complex formation using BiFC. (A) S2 cells co-transfected with Actin-Gal4 + UAS-RFP (to mark transfected cells) and the indicated expression constructs (e.g. UAS-NYFP + UAS-NYFP) were DAPI stained and imaged using epifluorescence microscopy to assay for YFP reassembly (BiFC signal). (B) Co-expression of UAS-NYFP-Rop and UAS-Sec6-CYFP under control of the epidermal A58-Gal4 driver, but not expression of UAS-NYFP-Rop alone, results in YFP fluorescence in the body wall, indicative of Rop-Sec6 complex formation. YFP fluorescence is enriched at cell-cell junctions (dashed line). (C) Dendritic morphologies of representative wild-type, *Sec6*^{Δ20}, or *Sec6*^{Δ20} + *UAS-Sec6-CYFP* C4da-ddaC MARCM clones. Scale bar, 100 μm. (D,E) Mean and standard deviation of total dendrite length (D) and terminal dendrite number (E) is shown, with the number of neurons analyzed for each genotype indicated. Bars represent mean values *** *p* < 0.001, ns, not significant, compared to wild type controls (one-way ANOVA with Tukey's HSD *post hoc* analysis).